JGR Oceans

RESEARCH ARTICLE
10.1029/2020JC016486

Special Section:
The Arctic: An AGU Joint Special Collection

Structure of the Freshened Surface Layer in the Kara Sea During Ice-Free Periods

A. A. Osadchiev[1,2,3,4], D. I. Frey[1], S. A. Shchuka[1,2], N. D. Tilinina[1], E. G. Morozov[1], and P. O. Zavialov[1]

[1]Shirshov Institute of Oceanology, Russian Academy of Sciences, Moscow, Russia, [2]Institute of Geology of Ore Deposits, Petrography, Mineralogy and Geochemistry, Russian Academy of Sciences, Moscow, Russia, [3]Moscow Institute of Physics and Technology, Dolgoprudny, Russia, [4]National Research Tomsk State University, Tomsk, Russia

Key Points:

- Large low-salinity and stratified freshened surface layer is formed in the Kara Sea during short-term flooding period in early summer
- Area and position of this freshened layer remain stable till the end of the ice-free period, while its vertical structure largely changes
- Formation of the seasonal halocline occurs during summer and autumn at the stable area in the central Kara Sea

Supporting Information:

- Supporting Information S1

Correspondence to:
A. A. Osadchiev,
osadchiev@ocean.ru

Citation:
Osadchiev, A. A., Frey, D. I., Shchuka, S. A., Tilinina, N. D., Morozov, E. G., & Zavialov, P. O. (2021). Structure of the freshened surface layer in the Kara Sea during ice-free periods. *Journal of Geophysical Research: Oceans*, *126*, e2020JC016486. https://doi.org/10.1029/2020JC016486

Received 6 JUN 2020
Accepted 9 NOV 2020

Abstract This work is focused on the seasonal and interannual variability of the freshened surface layer (FSL) in the Kara Sea during ice-free periods. The majority of annual freshwater runoff inflows to the Kara Sea during the freshet period in June–July. As a result, a large low-salinity and strongly stratified FSL is formed in the central Kara Sea at the beginning of the ice-free period. Initially, this layer is fresh with salinities of less than 15. Then, in August–October, river discharge steadily decreases, the fresh (<15) and strongly stratified river plume remains limited to the inner part of the FSL adjacent to the Ob and Yenisei gulfs, which receives reduced freshwater discharge. The area of the fresh plume steadily decreases with decreasing of river discharge; in October, it remains only within the Ob and Yenisei gulfs. Area and position of the outer part of the FSL, on the opposite, remain stable until the end of ice-free period. Salinities in the outer part steadily increase to 20–25, vertical salinity gradients at the boundary with the subjacent sea decrease, albeit remain prominent. Area and position of the FSL also have low interannual variability, because the volume of river runoff during freshet period in June–July is stable on interannual time scale. As a result, downward freshwater transport and the formation of the seasonal halocline occur in August–October at the stable area located in the central Kara Sea.

Plain Language Summary The Arctic Ocean receives enormous continental runoff, as compared to the other oceans. This freshwater discharge forms large freshened water masses on the Arctic shelf that plays a crucial role in variability of ice cover and regional albedo. These water masses significantly affect physical, biological, and geochemical processes in the Arctic, especially, in coastal and shelf areas where impact of freshwater discharge is the strongest. The Kara Sea contains the largest amount of freshwater among the basins of the Arctic Ocean. It receives approximately a quarter of the Arctic freshwater runoff from the Ob and Yenisei rivers. In this study, we address the fate of freshwater discharge in the Kara Sea during ice-free periods. We reveal that this process consists of two subsequent stages, namely, horizontal advection and vertical mixing. Initially, the thin and low-salinity surface layer quickly spreads over wide area in the Kara Sea during flooding river discharge in June–July. Then river discharge drops, expanding of this layer slows down, and it steadily mixes with subjacent sea. As a result, downward freshwater transport and formation of seasonal halocline occurs in August–October at the stable area located in the central Kara Sea.

1. Introduction

The Kara Sea is a semi-enclosed sea located between the Siberian coast in the south, Novaya Zemlya in the west, and Severnaya Zemlya in the east (Figure 1). The water depth is less than 50 m at more than 40% of the Kara Sea; shallow areas are located mainly in the central and south-eastern parts of the sea. This sea receives enormous freshwater discharge (~1,500 km^3 annually) mainly from two large estuaries, namely, the Yenisei Gulf (630 km^3 from the Yenisei River) and the Gulf of Ob (530 km^3 from the Ob, Pur, and Taz rivers; Gordeev et al., 1996; Pavlov et al., 1996). Continental discharge to the Kara Sea has very large seasonal variability with a short freshet period in June–July that provides ~50% of annual runoff and a long low discharge period in October–April caused by freezing of the inflowing rivers (Pavlov et al., 1996; Figure 1).

Freshwater discharge forms the large freshened surface layer (FSL) in the Kara Sea which is among the largest freshwater reservoirs in the Arctic Ocean (Aagaard & Carmack, 1989; Haine et al., 2015; Williams

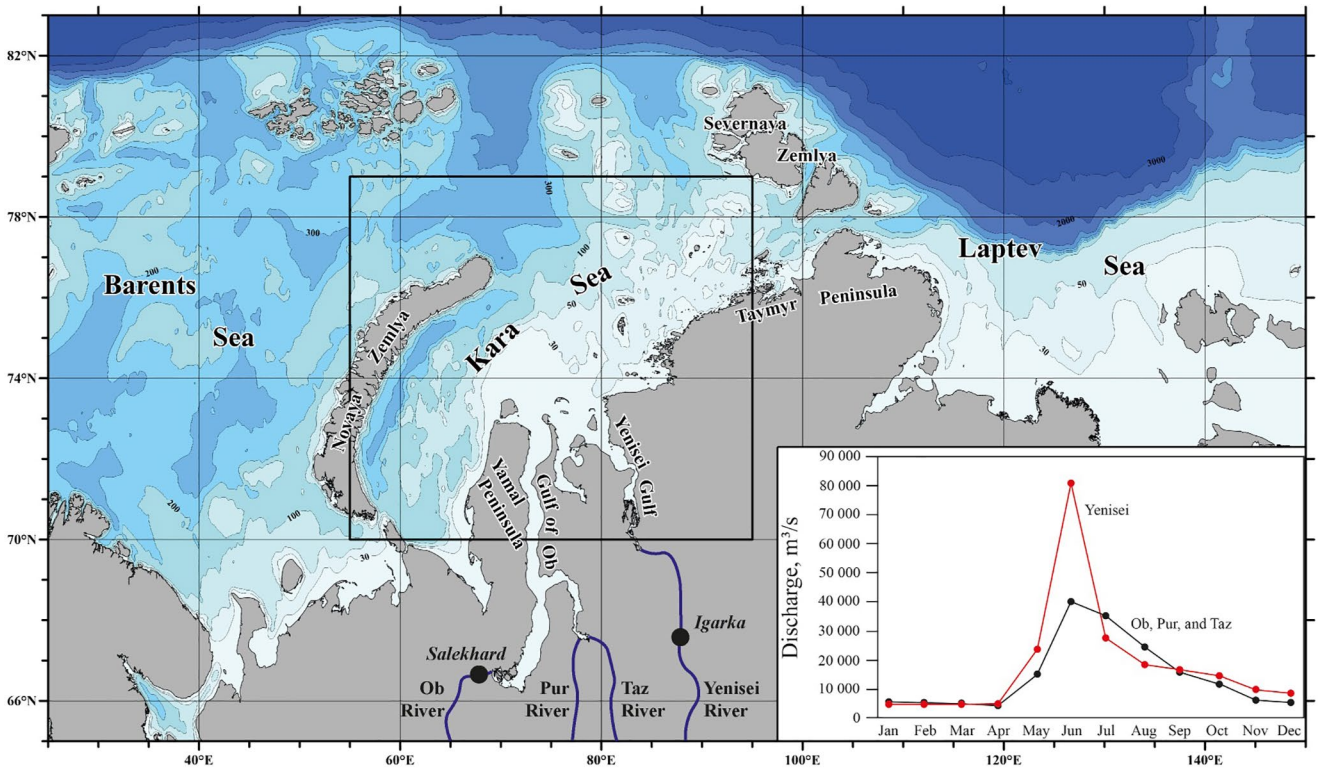

Figure 1. Study area, location of gauge stations at the Ob, and Yenisei rivers in Salekhard and Igarka (black circles), and mean annual hydrographs of the Ob (with Pur and Taz) and Yenisei rivers. The black box indicates the area shown in Figures 2, 5, 8, and 9.

& Carmack, 2015) and governs many local physical, biological, and geochemical processes (Asadulin et al., 2013, 2015; Dubinina et al., 2017a, 2017b; Galimov et al., 2006; Gebhardt et al., 2004; Kohler et al., 2003; Levitan et al., 2005; Makkaveev et al., 2015; Miroshnikov, 2013; Mosharov et al., 2018a, 2018b; Osadchiev et al., 2017, 2020; Polukhin, 2019; Romanova & Boltenkova, 2020; Unger et al., 2005). Many previous studies addressed water masses, inflow of warmer water from the Barents Sea, and circulation in the Kara Sea (Dmitrenko et al., 2015; Harms & Karcher, 1999, 2005; McClimans et al., 2000; Morozov et al., 2003, 2008; Osadchiev et al., 2020b; Panteleev et al., 2007; Pavov & Pfirman, 1995; Zatsepin, et al., 2010a). However, only limited studies were focused on the structure of FSL in the Kara Sea and they were based on in situ data collected during individual field works conducted in September (Johnson et al., 1997; Osadchiev et al., 2017; Zatsepin et al., 2010b, 2015; Zavialov et al., 2015). As a result, the seasonal and interannual variability of spatial extent and vertical structure of FSL during the majority of the year remains largely unknown.

The process of transformation of freshwater discharge as a result of its interaction with saline sea water can be considered and analyzed on different spatial and temporal scales. Initially, river discharge enters the shelf sea from a river mouth and forms a submesoscale (with spatial extents ~1–10 km) or mesoscale (with spatial extents ~10–100 km) water mass commonly referred to as a river plume. Salinity within a plume is significantly lower than that of surrounding sea water (Horner-Devine et al., 2015; Osadchiev & Zavialov, 2019). Structure and dynamical characteristics within a river plume are strongly inhomogeneous. In particular, salinity and velocity fields in the vicinity of a freshwater source are significantly different as compared to the outer parts of a plume (Fong & Geyer, 2002; Horver-Devine et al., 2015; Osadchiev, 2018; Osadchiev et al., 2016; Osadchiev & Sedakov, 2019). A river plume is spreading and mixing with ambient saline sea water, which results in the transformation of a plume, but also influences the hydrological structure of the ambient sea. Strength and extent of this influence mainly depend on the volume of freshwater discharge and varies from negligible impact of small plumes formed by rivers with low discharge rates (Korotkina et al., 2011, 2014; Osadchiev, 2015; Osadchiev et al., 2020d; Ostrander et al., 2008; Romero et al., 2016) to the formation of stable freshened water masses in the upper ocean by the world's largest rivers on wide coastal and shelf areas (Denamiel et al., 2013; Geyer et al., 1996; Lentz, 1995; Schiller et al., 2011) as is the

case of the Ob-Yenisei plume in the Kara Sea (Osadchiev, 2017; Osadchiev et al., 2020a). The latter water masses with spatial extents on the order of hundreds of kilometers are commonly referred to as regions of freshwater influence (ROFI). These water masses are characterized by rather homogenous structure, significantly greater spatial scales, and lower temporal variability, as compared to river plumes. Thus, we divide the continuous process of transformation of freshwater discharge into two stages, namely, transformation on diurnal (approximately several hours) to synoptic (approximately several weeks) time scales within river plumes and transformation on seasonal (approximately several months) to annual time scales within ROFI's (for rivers which are large enough to form ROFI's; Osadchiev & Zavialov, 2019).

This study continues our previous research of river plumes and ROFI's in the Kara Sea focused on the structure of the Ob-Yenisei plume (Osadchiev et al., 2020a), interaction between the Ob- and Yenisei-dominated parts of the Ob-Yenisei plume (Osadchiev et al., 2017, 2019), and spreading of the Kara ROFI to the Laptev Sea through the Vilkitsky Strait (Osadchiev et al., 2020b). In the current study, we focus on the formation and transformation of large-scale FSL in the Kara Sea. We report in situ measurements performed in the Kara Sea during 11 field surveys conducted from July to October in different years. Based on these data and satellite observations of the Kara Sea, we study the fate of freshwater discharge in the Kara Sea during ice-free periods. The paper is organized as follows. Section 2 provides detailed information about the in situ, satellite, river discharge, and atmospheric reanalysis data used in this study. Section 3 describes external forcing conditions in the study area during ice-free season, as well as the vertical structure and spatial extents of FSL in the Kara Sea based on in situ and satellite data. Seasonal transformation of FSL including interaction between the Ob-Yenisei plume and the Kara ROFI, as well as interannual variability of this process are analyzed and discussed in Section 4 followed by the conclusions in Section 5.

2. Data

Hydrographic in situ data used in this study were collected during 11 oceanographic surveys in the Kara Sea onboard the research vessels "Akademik Mstislav Keldysh" and "Professor Shtokman" in 2007, 2011, and 2013–2019 (Table 1). The field surveys included continuous measurements of salinity in the sea surface layer (2–3-m depth) performed along the ship track (Figure 2, lines) using a ship board pump-through system equipped with a thermosalinograph (*SBE 21 SeaCAT*). In 2007, 2011, 2014, and 2016, the vertical thermohaline structure was measured at hydrographic stations along two quasi-meridional transects, namely, from the northern part of the Gulf of Ob to the latitude of ~76.5°N (hereafter, referred as the Ob transect)

Table 1
Periods, Research Vessels, Areas, and Types of In situ Measurements of Oceanographic Surveys

Periods	Research vessel	Type of in situ measurements
September 2007	Akademik Mstislav Keldysh	Continuous measurements and hydrographic stations at the Ob transect (23–30 September)
September 2011	Akademik Mstislav Keldysh	Continuous measurements and hydrographic stations at the Yenisei transect (18–23 September)
September 2013	Professor Shtokman	Continuous measurements
August 2014	Professor Shtokman	Continuous measurements and hydrographic stations at the Yenisei (17–28 August) and Ob (22–23 August) transects
September–October 2015	Akademik Mstislav Keldysh	Continuous measurements
July 2016	Akademik Mstislav Keldysh	Continuous measurements and hydrographic stations at the Yenisei (18–21 July) and Ob (24–25 July) transects
September 2017	Akademik Mstislav Keldysh	Continuous measurements
August–September 2018	Akademik Mstislav Keldysh	Continuous measurements
September–October 2018	Akademik Mstislav Keldysh	Continuous measurements
July 2019	Akademik Mstislav Keldysh	Continuous measurements
September–October 2019	Akademik Mstislav Keldysh	Continuous measurements

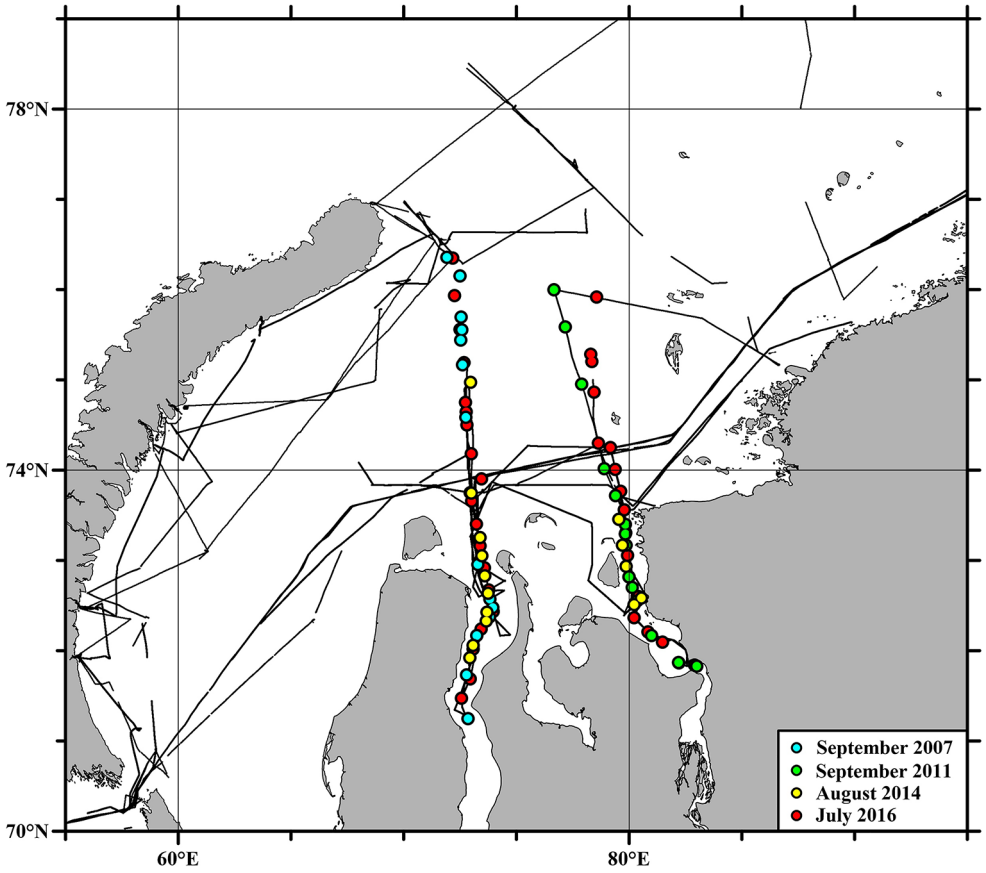

Figure 2. Continuous measurements along the ship tracks (black lines) of 11 oceanographic field surveys conducted in the Kara Sea and location of hydrographic stations conducted in September 2007 (green circles), August 2014 (yellow circles), and July 2016 (red circles).

and from the northern part of the Yenisei Gulf to the latitude of ~76°N (hereafter, referred as the Yenisei transect; Figure 2, circles). Vertical thermohaline structure was measured using a CTD instrument (*SBE 911plus*) at 0.2-m spatial resolution. This CTD profiler was equipped with two parallel temperature and conductivity sensors; the mean temperature differences between them did not exceed 0.01°C, while that of salinity was not greater than 0.01 PSU.

Wind forcing conditions were examined using ERA5 atmospheric reanalysis with a 0.25° spatial and hourly temporal resolution. Discharge data used in this study were obtained at the downstream-most gauge stations at the Ob and Yenisei rivers in Salekhard and Igarka (Figure 1). Satellite data used in this study include Terra/Aqua Moderate Resolution Imaging Spectroradiometer (MODIS) satellite imagery. MODIS L1b calibrated radiances including MODIS bands 1 (red), 3 (blue), 4 (green), and daytime 31 (thermal) were processes by ESA BEAM software to retrieve maps of sea surface distributions of corrected reflectance, concentration of chlorophyll-a (Chl-a), and brightness temperature at the study area with spatial resolutions of 500 m, 500 m, and 1 km, respectively. Chl-a distributions were calculated using the Ocean Color 3M algorithm (O'Reilly et al., 1998; Werdell & Bailey, 2005).

3. Results

3.1. Atmospheric Forcing, River Discharge, and Ice Conditions

Freshwater balance in the semi-enclosed Kara Sea is governed by river discharge and ice melt. Precipitation and evaporation play insignificant roles in freshwater balance in the Kara Sea, as well as in the Arctic Ocean in general due to the large sea ice cover and low air temperatures (Lambert et al., 2019). Daily averaged air

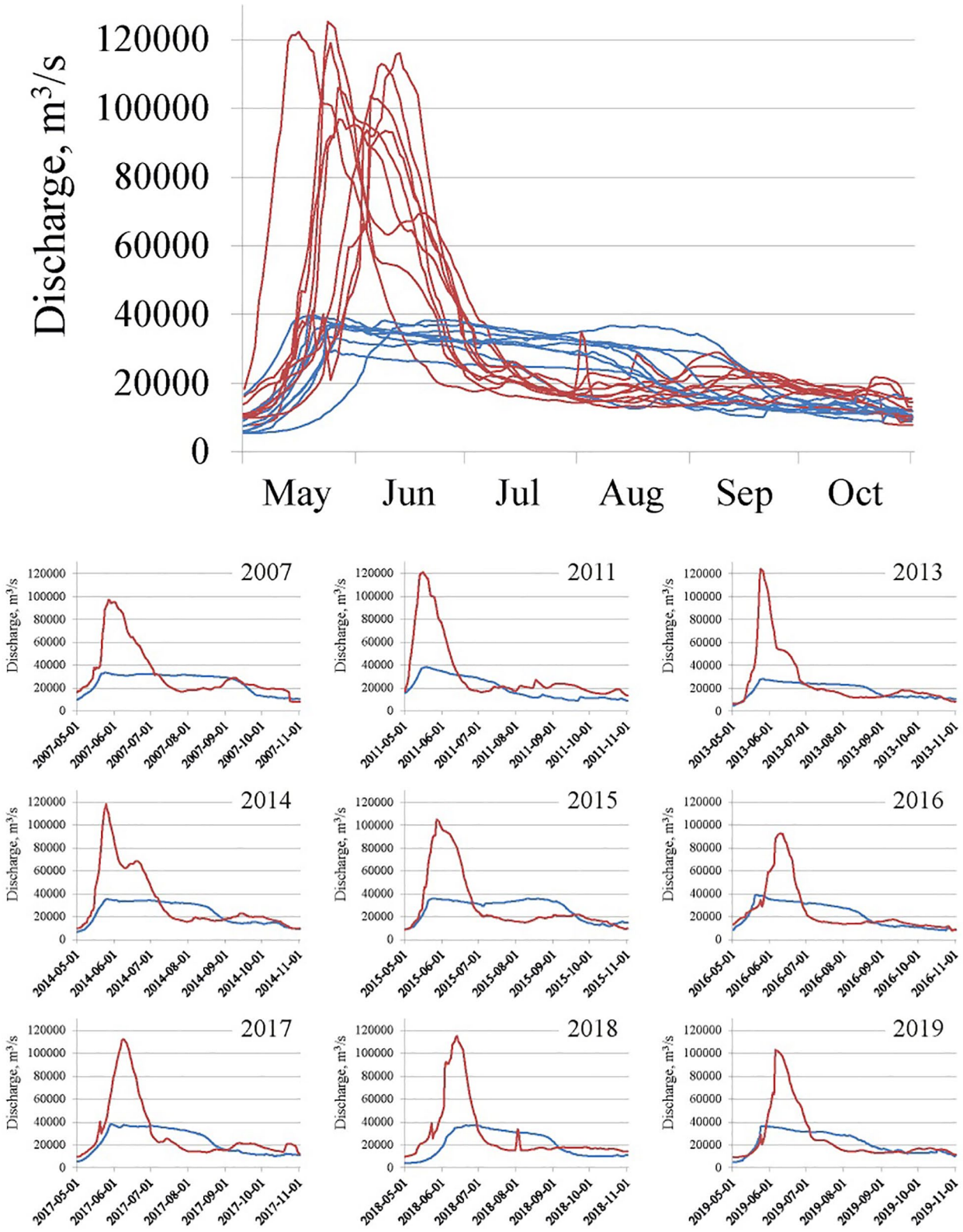

Figure 3. Discharge rates of the Ob (blue lines) and Yenisei (red lines) rivers in May–October measured at the gauge stations in Salekhard and Igarka during the years of oceanographic field surveys in the Kara Sea in 2007, 2011, and 2013–2019. Top panel shows discharge rates during all considered years and bottom panels show discharge rates during individual years.

temperatures in the central Kara Sea are <5°C during the whole year including the summer period (Pavlov et al., 1996). Annual precipitation in the central Kara Sea is 250–400 mm, with the majority provided during the cold ice-covered season (Pavlov et al., 1996).

The Kara Sea is frozen during the majority of the year. The southern part of the sea adjacent to the Ob and Yenisei gulfs is covered by landfast ice (~2-m thick) from November to the end of July (Pavlov et al., 1996; Pavlov & Pfirman, 1995). However, during certain years intense ice melt occurs several weeks earlier, that is, at the end of June and beginning of July. In particular, sea ice was already almost absent in the study area on July 15 in 2007, July 12 in 2011, July 7 in 2015, July 12 in 2016, July 9 in 2019. The summer freshet discharge of relatively warm water from the Ob and Yenisei gulfs accelerates break-up of the landfast ice and transport of ice floes to the northern Kara Sea. The analysis of isotope characteristics of FSL in the Kara Sea revealed that its volume is composed of river water directly mixed with saline sea water (Dubinina et al., 2017a, 2017b). As a result, during late summer and autumn, large river discharge determines the freshwater balance in the central Kara Sea, while the contribution of sea ice melt to FSL is negligible.

Figure 3 shows hydrographs, that is, daily discharge rates, of the Ob and Yenisei rivers during ice-free periods of the years of oceanographic field surveys in the Kara Sea. Discharge conditions during these years show large seasonal and low interannual variability. Yenisei River discharge is characterized by a distinct freshet in May–June (up to 100,000–120,000 m^3/s) followed by steady decrease of discharge in July–September (10,000–20,000 m^3/s) and a low discharge period in October–May (5,000–10,000 m^3/s; Figure 3). Seasonal variability of the Ob River discharge is flattened by dams located at the river and its large tributaries. As a result, the Ob River has less prominent high discharge from May/June to August/September (20,000–40,000 m^3/s) and a low discharge period from October to April/May (5,000–10,000 m^3/s; Figure 3).

In this study, we analyze the seasonal variability of the vertical structure of FSL in the Kara Sea using in situ measurements performed in July, August, and September. However, these measurements were conducted during different years, namely, in July 2014, August 2014, September 2007, and September 2011. Therefore, these measurements are indicative of seasonal variability of FSL only in case of similar external forcing conditions during these years, which causes low interannual variability of FSL among these years. The main external conditions that govern formation, spreading, and mixing of FSL are, first, freshwater discharge from the Ob and Yenisei gulfs and, second, wind forcing in the Kara Sea (Harms & Karcher, 2005; Osadchiev et al., 2017; Panteleev et al., 2007).

The analyzed river discharge measurements were performed in the downstream-most gauge stations at the Ob and Yenisei rivers. However, in this study we address the spreading of river discharge, which enters the Kara Sea from the estuaries of the Ob and Yenisei rivers. Therefore, we have to analyze the timing of runoff entering the sea and not the timing of runoff entering the large river estuaries. The distances between the Salekhard/Igarka and the mouths of the Ob/Yenisei gulfs are ~1,000/800 km. Therefore, we shifted the hydrographs measured in Salekhard and Igarka by 48 and 35 days onwards to obtain the hydrographs at the mouths of the Ob and Yenisei gulfs according to estimates of the flow speed in the Ob and Yenisei gulfs (0.3 m/s; Dolgopolova, 2015; Harms & Karcher, 1999; Panteleev et al., 2007) and in the Yenisei River (0.45 m/s; Semizhon et al., 2010). The resulting total runoff volumes from the Ob and Yenisei gulfs during May–September in 2007, 2011, 2014, 2016 reveal that river discharge conditions preceding the periods of field measurements in July 2016, August 2014, September 2007, and September 2011 were similar to long-term mean values (Figure 4). The early discharge peak, which occurred in the end of June 2011, is likely to cause earlier formation of FSL; however, total river runoff in May–September 2011 (706 km^3) was similar to the long-term average value (688 km^3). Therefore, we presume that the structure of FSL returned to typical conditions at the period of field measurements on 23–30 September 2011.

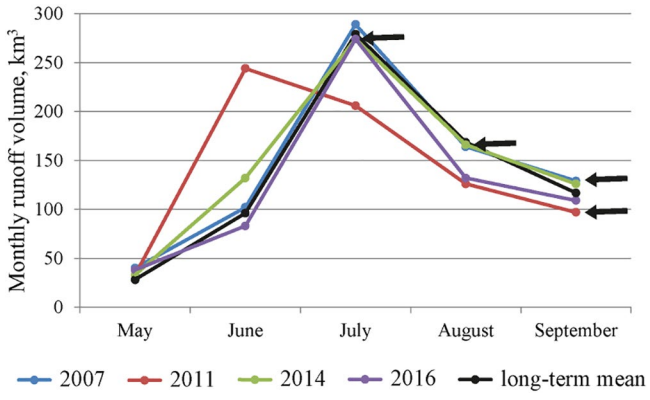

Figure 4. Total monthly runoff volumes from the Ob and Yenisei gulfs during May–September in 2007, 2011, 2014, 2016, as well as the related long-term mean values. The black arrows indicated periods of oceanographic field surveys in the Kara Sea in July 2016, August 2014, September 2007, and September 2011.

Wind forcing conditions from the beginning of the ice-free season until the time of the oceanographic field surveys in July 2016, August 2014,

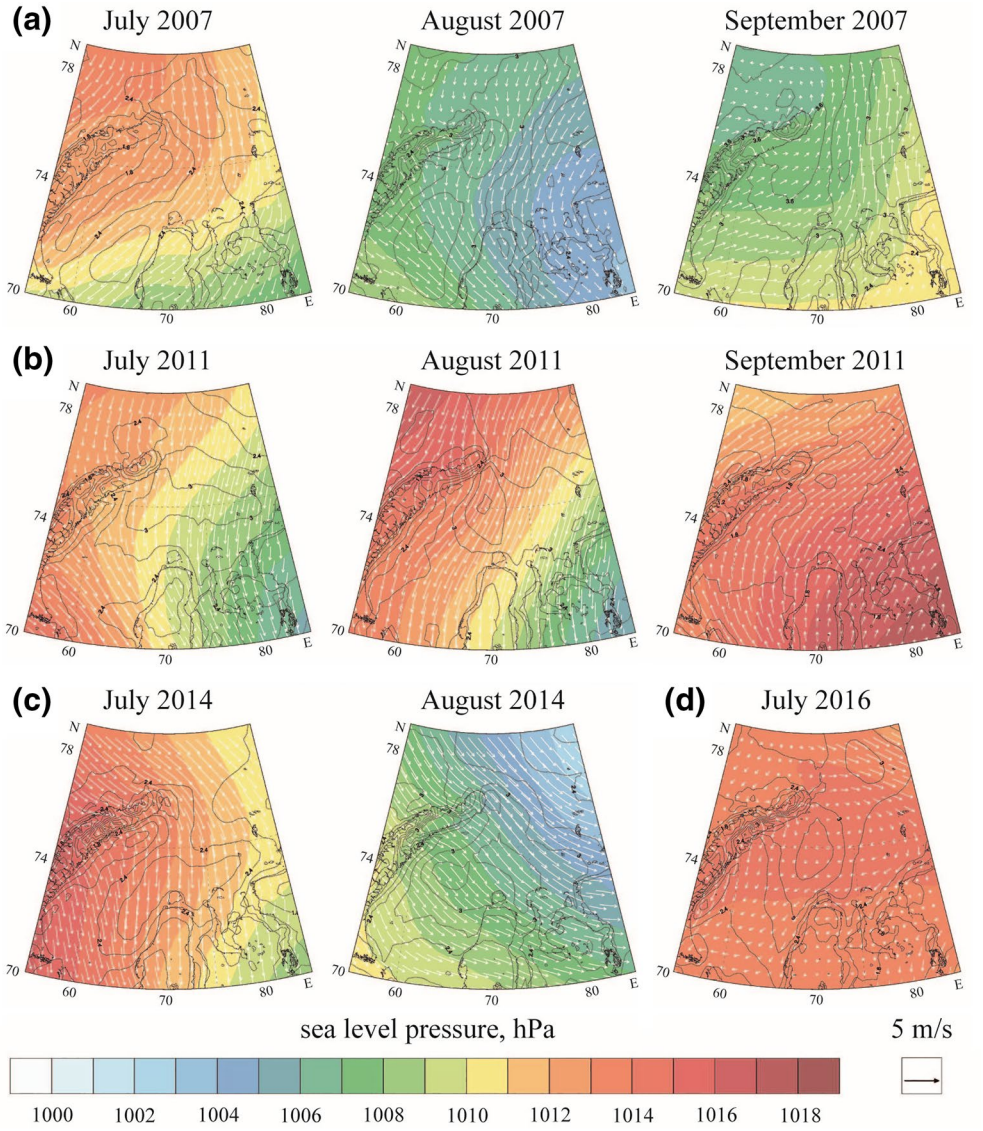

Figure 5. Monthly averaged wind forcing (arrows), standard deviation of wind speed (contours), and sea level pressure (color) in the central Kara Sea in (a) July–September 2007, (b) July–September 2011, (c) July–August 2014, and (d) July 2016, that is, from the beginning of the ice-free season till the periods of oceanographic field surveys.

September 2007, and September 2011 are shown in Figure 5. Northerly winds dominated in the study area in July and August during these years, with wind speeds of 3–6 m/s during the majority of these periods. In September 2007 and 2011, this atmospheric circulation pattern changed to southerly and south-westerly winds, while their average speed remained moderate. Monthly averaged wind speed was 2–3 m/s in August and September 2007, September 2011, July 2014, and July 2016. In July 2007, July and August 2011, and August 2014, the average wind speed was 4–5 m/s. As a result, wind forcing conditions in 2007, 2011, 2014, and 2016 were similar and moderate during the considered periods, standard deviation does not exceed 3 m/s. Therefore, we presume low interannual variability in the formation and spreading of FSL in the Kara Sea during these years.

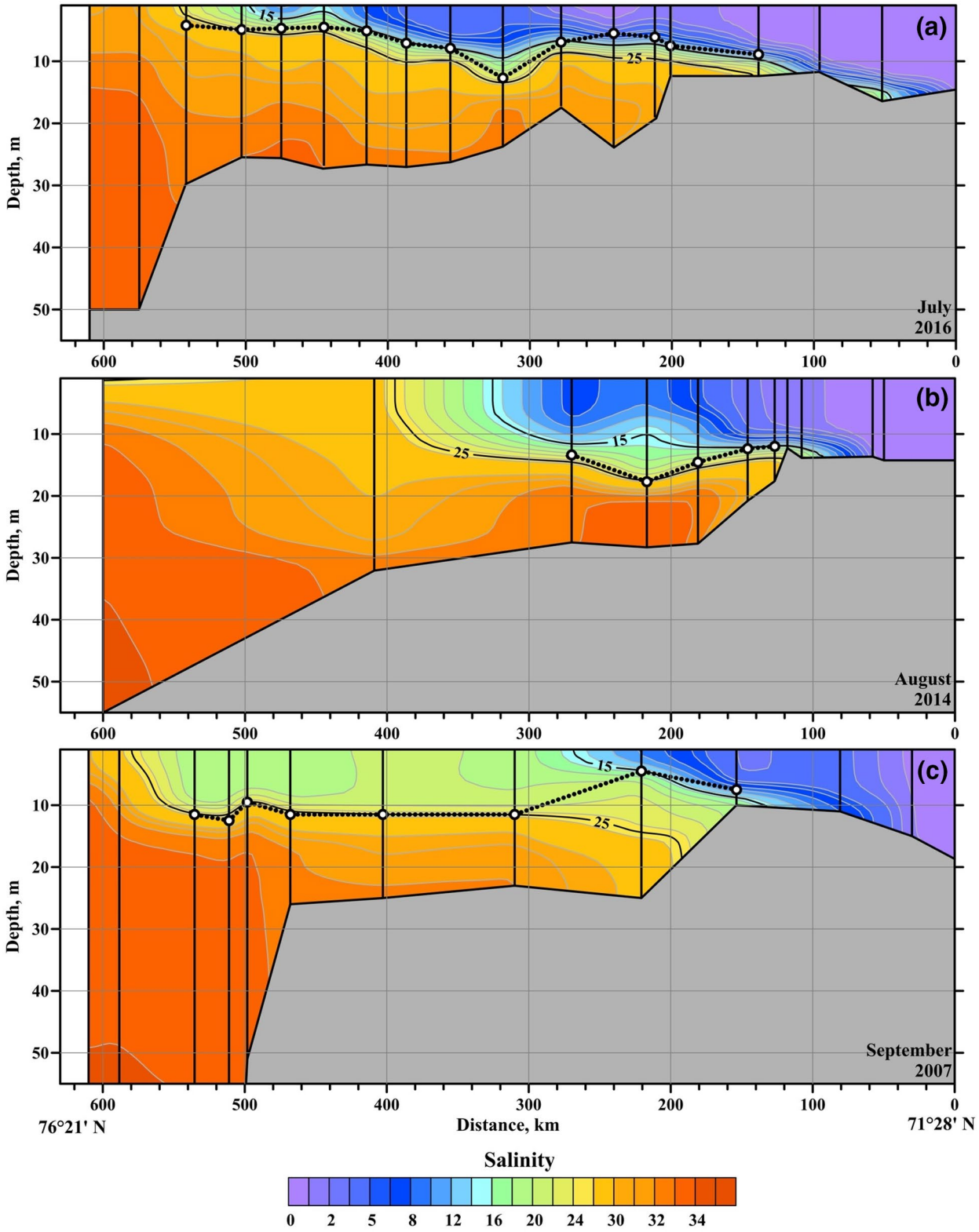

Figure 6. The vertical salinity structure along the Ob transect in the Kara Sea on (a) July 18–21, 2016, (b) August 17–28, 2014, and (c) September 23–30, 2007. The isohalines of 15 and 25 are shown by bold lines. White circles indicate locations of the maximal values of vertical salinity gradient at the vertical profiles. Location of the Ob transect is shown in Figure 2 by colored circles.

3.2. Vertical Structure of FSL

The vertical structure of FSL in the Kara Sea was studied based on vertical temperature and salinity measurements performed at hydrographic stations along the Ob transect in September 2007, August 2014, and July 2016 and at hydrographic stations along the Yenisei transect in September 2011, August 2014, and July 2016 (Figure 2). These sections cross the central FSL and are representative of its vertical structure. Figures 6–9 show large differences among the vertical thermohaline structure of FSL observed in July, August, and September.

In July 2016, the FSL was shallow (5–10-m deep) and fresh with salinities of less than 15 (Figures 6a and 8a) and temperatures of 8°–10°C (Figures 7a and 9a). Sharp salinity gradients were formed at the boundary between FSL and the subjacent sea. Maximal values of vertical salinity gradients were observed at the isohalines of 14–16 from the estuaries reaching as far as 400–500-km north along the transects. Further northward maximal gradients shifted to the isohalines of 24–26 in the northernmost part of FSL. In August 2014, surface salinities of <15 were observed only until 350 km into the Ob transect. Vertical salinity gradients at the bottom boundary of FSL relaxed outside the estuaries, while the depth of FSL increased to 13–18 m as a result of mixing with saline sea water (Figures 6b and 7b). The temperature of FSL reduced to 4°–7°C (Figures 7b and 9b). Maximal values of vertical salinity gradients shifted from the isohalines of 14–16 within the estuaries to the isohalines of 20–25 in the central Kara Sea. In September 2007 and September 2011, FSL was less fresh as a result of mixing under decreased river discharge conditions. The salinities of the majority of volume of FSL increased to 20–25 (Figures 6c and 8c), while its temperature decreased to 1°–3°C in 2007 (Figure 7c) and 4°–5°C in 2011 (Figure 9c). Surface salinity <15 and temperature >6°C were limited to the southern parts of the transects within the Ob and Yenisei gulfs (Figures 6c, 7c, 8c, and 9c). The depth of FSL was also reduced to 5–10 m. Maximal values of vertical salinity gradients were registered at the isohalines of 14–16 in the southern part of the transects and at the isohalines of 24–26 in the central and northern parts of the transects.

The vertical thermohaline structure of FSL described above shows that the low-salinity water mass constantly occupied the region inside and adjacent to the Ob and Yenisei gulfs. During the peak freshwater discharge in July, this water mass spread over large area in the central Kara Sea. In August–September, it was reduced to the region adjacent to the estuaries. Therefore, we associate this water mass with the Ob-Yenisei river plume, which represents the transformation of freshwater discharge on synoptic time scales (i.e., several weeks). The Ob-Yenisei plume is bounded by a distinct salinity gradient at the isohalines of 14–16, therefore, we determine its outer boundary by the isohaline of 15. The Ob-Yenisei plume is embedded into the shelf-wide Kara ROFI, which represents the transformation of freshwater discharge on seasonal time scales (i.e., several months). The Kara ROFI is not yet well-developed in July shortly after the beginning of the peak discharge. Then, in August, the Kara ROFI is formed in the northern part of FSL as a result of mixing between the Ob-Yenisei plume and the subjacent sea. In September, the Ob-Yenisei plume is totally transformed into the Kara ROFI in the open part of the Kara Sea. The Kara ROFI is bounded by a distinct salinity gradient at the isohalines of 24–26, therefore, we determine its outer border by the isohaline of 25.

The temperature-salinity diagram of the measurements along the Ob and Yenisei transects demonstrates the “linear” type of mixing between the warm and fresh river water and cold and saline sea water (Figure 10), that is, the dilution of the Ob-Yenisei plume and the Kara ROFI occurs as a result of entrainment of subjacent saline water to FSL. Temperature of river water steadily decrease from >15°C in July to 5°–10°C in September for the Yenisei River and from 6°–15°C in July to 5°–6°C in September for the Ob River.

3.3. Spatial Extents of FSL

In order to assess spatial extents of FSL in the Kara Sea, we analyzed in situ salinity measurements in the surface layer performed during field surveys referred above (Figures 11 and 12), as well as satellite observations of the study areas in 2000–2019 (Figure 13). Continuous in situ measurements of salinity in the surface layer are efficient to detect positions, shapes, and sizes of freshened water masses (Zavialov et al., 2018). Once the ship crosses the boundary of the Kara ROFI/Ob-Yenisei plume, salinity in the surface layer decreases below (or increases above) 25/15. Locations of the detected boundary segments provide

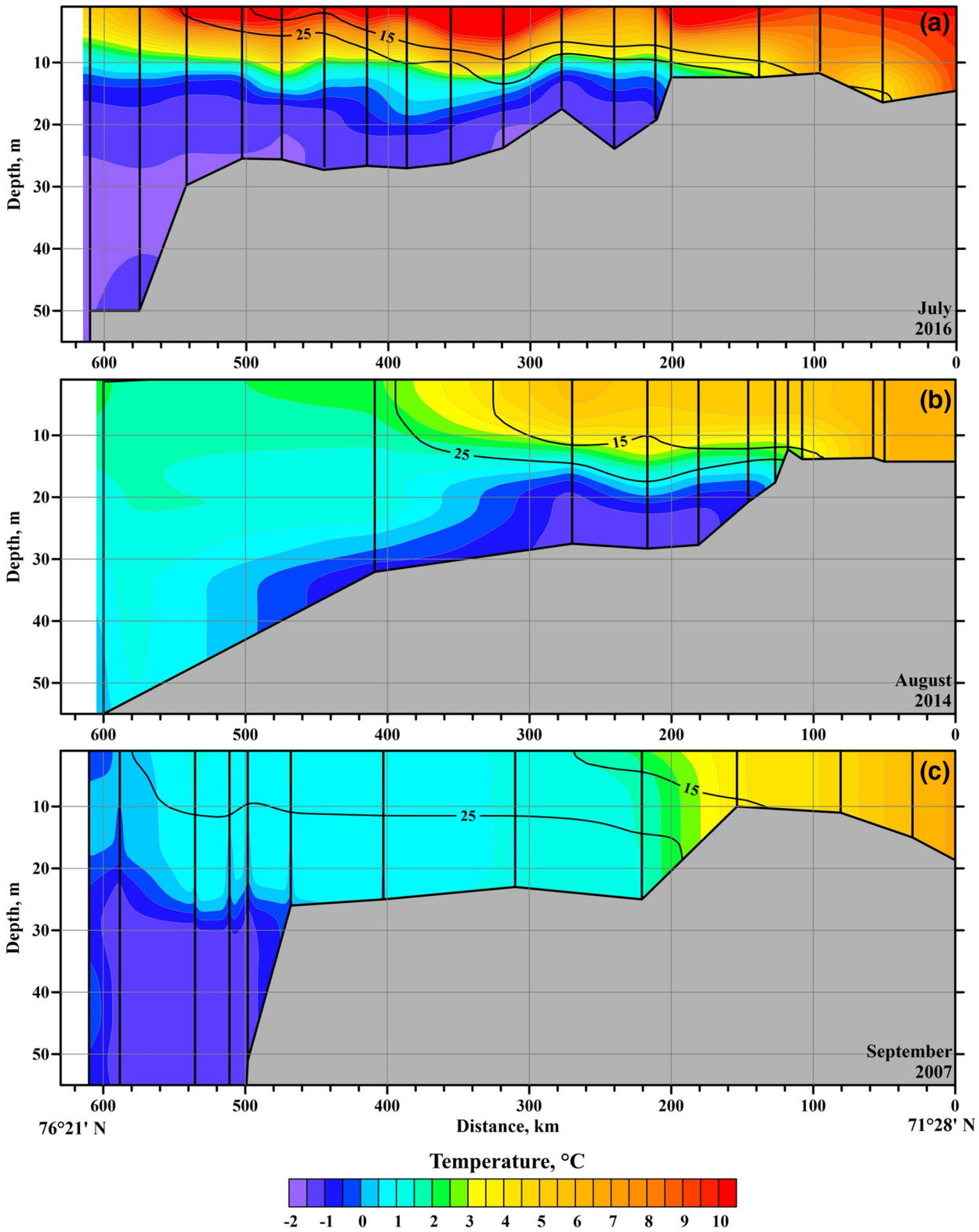

Figure 7. The vertical temperature structure along the Ob transect in the Kara Sea on (a) July 18–21, 2016, (b) August 17–28, 2014, and (c) September 23–30, 2007. The isohalines of 15 and 25 are shown by bold lines. Location of the Ob transect is shown in Figure 2 by colored circles.

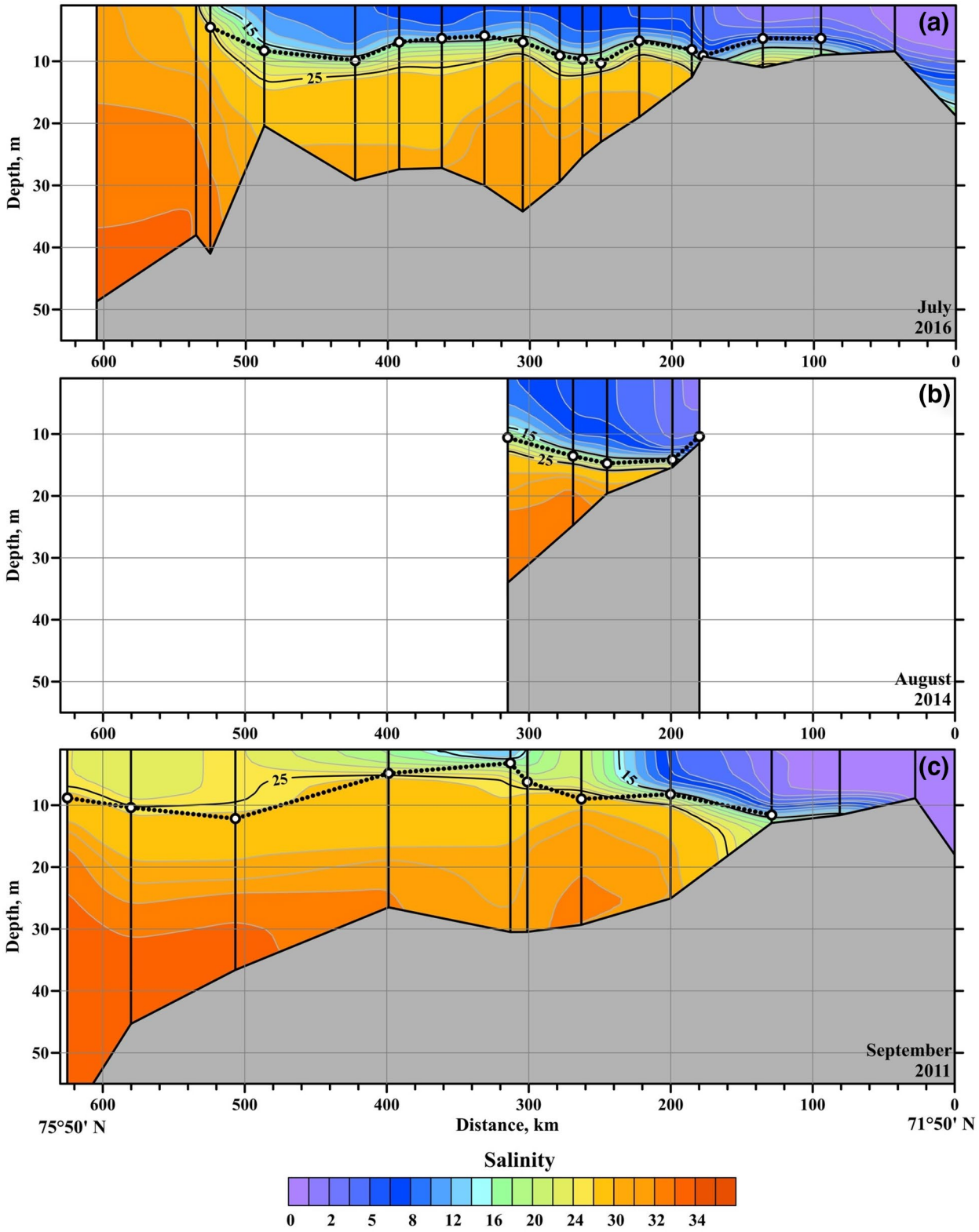

Figure 8. The vertical salinity structure along the Yenisei transect in the Kara Sea on (a) July 24–25, 2016, (b) August 22–23, 2014, and (c) September 18–23, 2011. The isohalines of 15 and 25 are shown by bold lines. White circles indicate locations of the maximal values of vertical salinity gradient at the vertical profiles. Location of the Yenisei transect is shown in Figure 2 by colored circles.

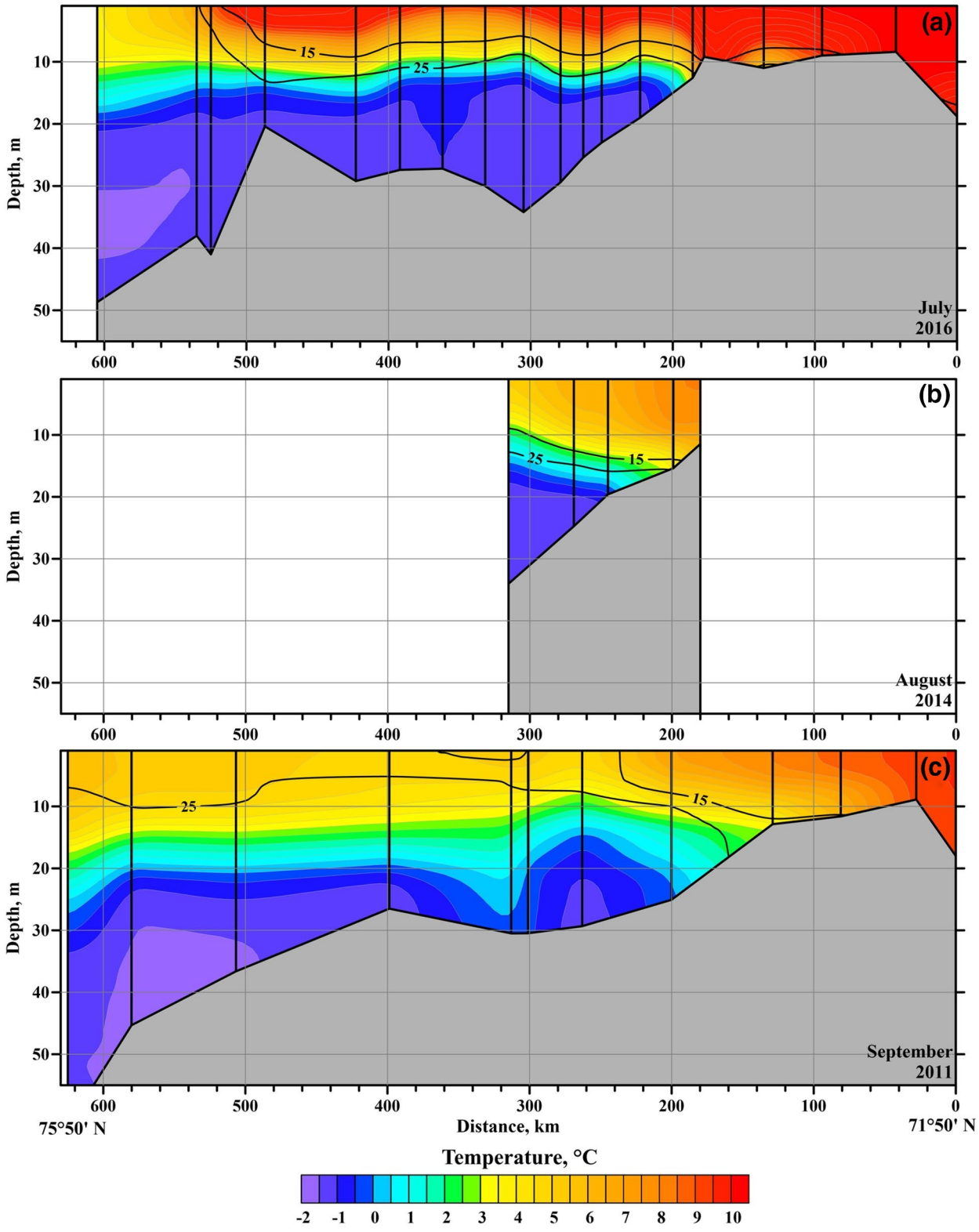

Figure 9. The vertical temperature structure along the Yenisei transect in the Kara Sea on (a) July 24–25, 2016, (b) August 22–23, 2014, and (c) September 18–23, 2011. The isohalines of 15 and 25 are shown by bold lines. Location of the Yenisei transect is shown in Figure 2 by colored circles.

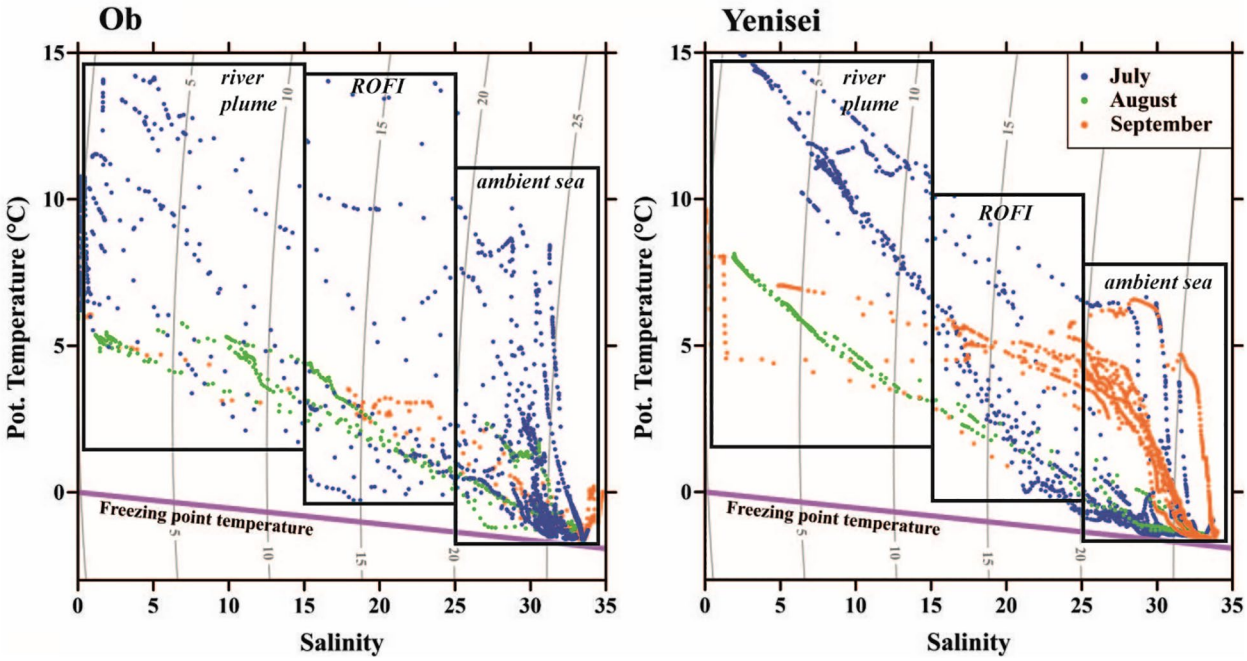

Figure 10. Temperature-salinity diagram including the freezing point temperature (magenta line) and sigma-contours (gray lines) at the hydrographic stations along the Ob (left) and Yenisei (right) transects in the Kara Sea in July (blue dots), August (green dots), and September (orange dots).

information about positions, shapes, and sizes of the Kara ROFI and the Ob-Yenisei plume. The ship tracks were distinct among the 11 surveys addressed in this study, which results in some bias of detection of spatial extents of the Kara ROFI and the Ob-Yenisei plume (Figure 2, black lines and Figure 11). However, their western, northern, and eastern boundaries were detected during the majority of the surveys. The western boundary of the Kara ROFI was detected in nine different surveys, the northern and eastern boundaries of the Kara ROFI were detected in seven different surveys, the western, northern, and eastern boundaries of the Ob-Yenisei plume were detected in six different surveys (Figure 12). As a result, the obtained data are representative of seasonal (June–October) and interannual (in September of different years) variability of spatial extents of the Kara ROFI and the Ob-Yenisei plume.

Based on in situ data, we reveal that the Kara ROFI (determined by the isohaline of 25) occupied relatively stable area in the central Kara Sea during the periods of 11 field campaigns conducted in 2007–2019 (Figure 12). At the south and east, the Kara ROFI was bounded by the Siberian coast, while its northern and western boundaries were located in the open sea between Novaya Zemlya and the Taymyr and Yamal peninsulas, respectively. In July (2016 and 2019) and August (2014 and 2018), the northern boundary of the Kara ROFI was located between the latitudes of 75°N-75.5°N (Figures 12a and 12b), while in September (2007, 2011, and 2015) it shifted northward to the latitudes of 76°N-77°N (Figure 12c). Positions of the eastern boundary of the Kara ROFI varied along the 150-km segment of the Taymyr Peninsula coast between the longitudes of 88°E-93°E. Positions of the western boundary of the Kara ROFI varied along the 250-km segment of the Yamal Peninsula coast between the latitudes of 71.5°E-73.5°E, and along the 150-km segment of the Novaya Zemlya coast between the latitudes of 74°N-75°N. The Ob-Yenisei plume, on the opposite, showed large variability of its shape and area. In July (2016 and 2019), the plume occupied wide area in the central Kara Sea. The northern boundary of the plume was located near the northern boundary of the Kara ROFI (Figure 12a). In August (2014), the northern boundary of the Ob-Yenisei plume shifted southward to the latitude of 74°N (Figure 12b). In September and October (2007, 2011, 2013, 2017, and 2018) surface salinities below 15 were registered only in the vicinity of and inside the Ob and Yenisei gulfs (Figures 12c and 12d). Thus, the meridional extent of the Ob-Yenisei plume decreased from 150 to 250 km in July–August to tens of kilometers in the semi-enclosed area between the Ob and Yenisei gulfs in late September–October.

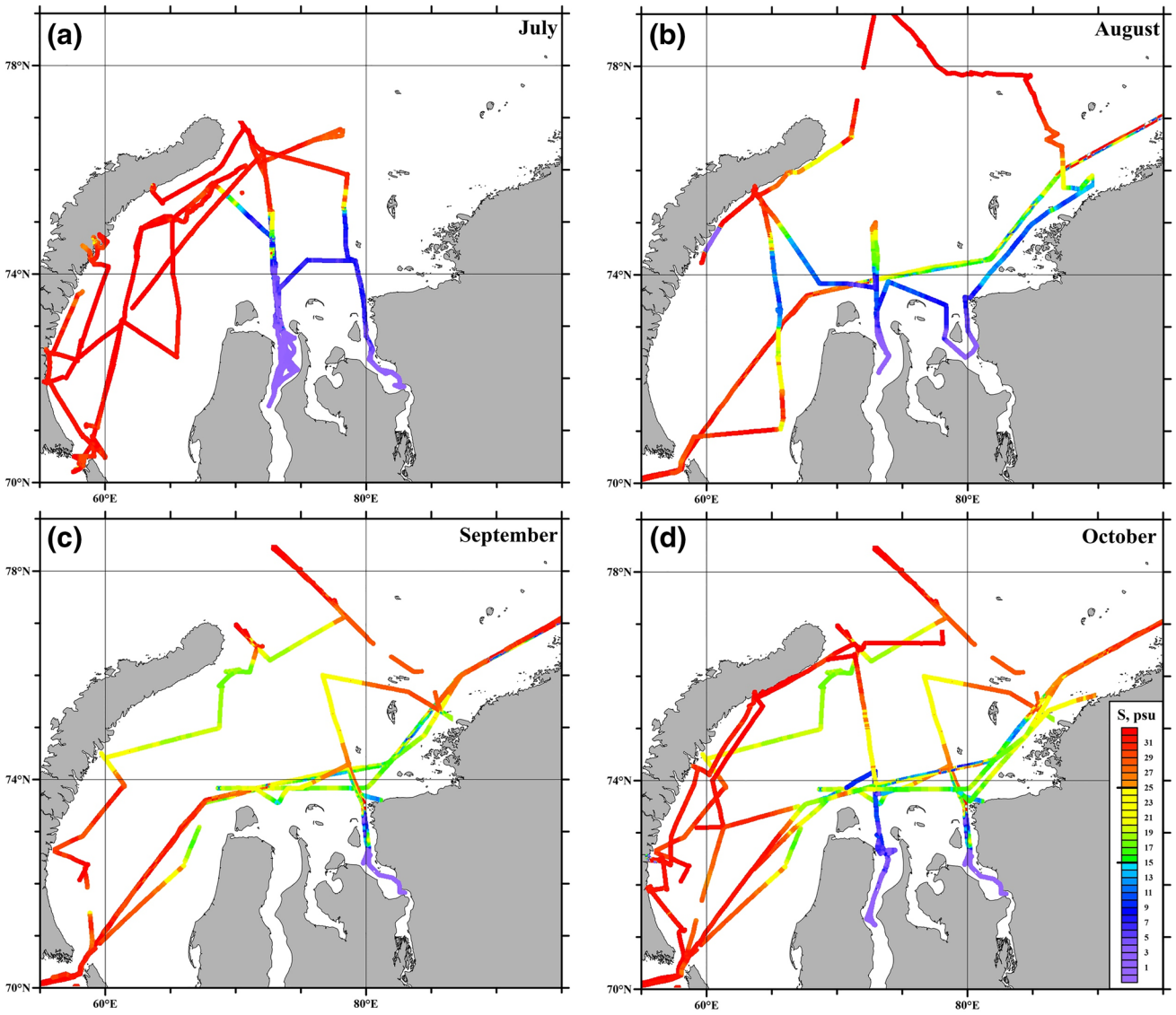

Figure 11. Salinity in the surface layer in the Kara Sea along the ship tracks during oceanographic field surveys in (a) July, (b) August, (c) September, and (d) October.

Several previous studies showed that elevated surface temperature and increased concentrations of Chl-a and CDOM are stable characteristics of FSLs in the Arctic Ocean, which form distinct frontal zones with cold and low-fluorescent ambient sea water (Fichot et al., 2013; Glukhovets & Goldin, 2014, 2020; Kubryakov et al., 2016; Osadchiev et al., 2020a, 2020b, 2020c). Lewis and Arrigo (2020) demonstrated that standard algorithms overestimate observed Chl-a concentrations in the shelf water in the Kara Sea that is caused by high concentrations of CDOM in riverine water. Therefore, satellite Chl-a maps do not correctly reproduce measured Chl-a concentrations in the study area. However, they do distinguish fresh riverine water (with high concentrations of both Chl-a and CDOM) from ambient sea water. As a result, they can be used to correctly determine the spreading area of FSL in the Kara Sea (Glukhovets & Goldin, 2014; Kubryakov et al., 2016).

The outer boundary of FSL in the Kara Sea was regularly observed in cloud-free images of the study area acquired in 2000–2019. As a result, the position and size of FSL are distinctly visible at corrected reflectance, brightness temperature, and Chl-a satellite images acquired during days when the whole central Kara Sea was free of clouds (Figure 13). The dashed lines in Figure 13, which illustrate locations of the outer

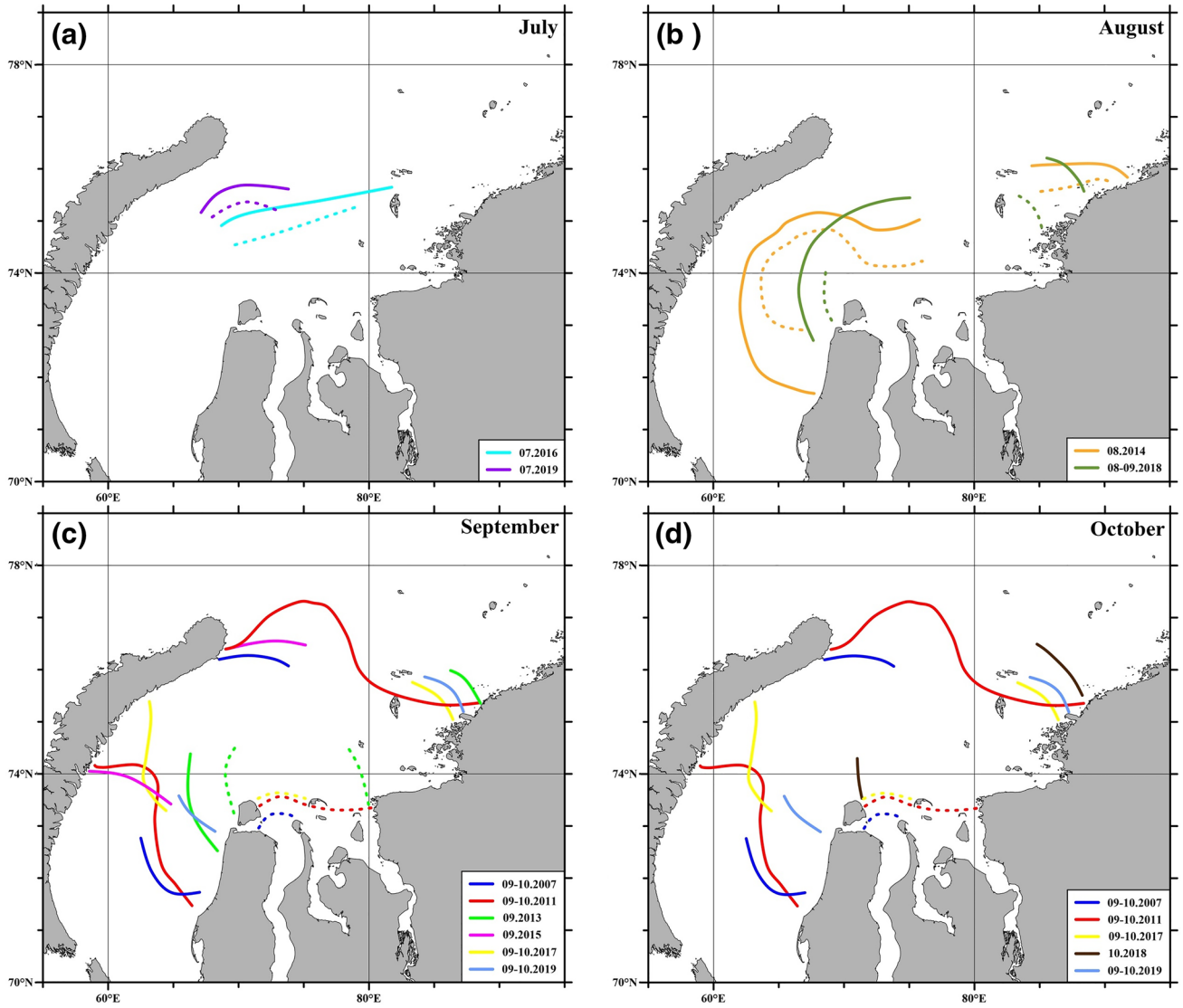

Figure 12. Locations of the isohalines of 15 (dashed lines) and 25 (solid lines) in the Kara Sea detected by continuous measurements along the ship tracks in (a) July, (b) August, (c) September, and (d) October.

boundary of FSL, correspond to Chl-a gradients in satellite maps, which border high satellite Chl-a concentrations (caused by high concentrations of both Chl-a and CDOM) within FSL. On the other hand, the Ob-Yenisei plume and the Kara ROFI cannot be accurately distinguished within FSL, because temperature and Chl-a gradients at their boundary are much smaller, as compared to the periphery of FSL.

Satellite imagery show that FSL in the Kara Sea has similar spreading patterns during different years in 2000–2019 that is consistent with in situ measurements. Seasonal variations of the position of the freshened layer were observed with satellite imagery during several years with relatively low cloud coverage including 2007, 2008, 2012, 2013, 2016, and 2019. Figure 13 illustrates variations of the position of FSL during the ice-free season in 2016, which is the most demonstrative example of this process and is also supported by in situ measurements. In June–July it occupies large area in the central Kara Sea, albeit its western and northern boundaries do not reach Novaya Zemlya. Satellite imagery reveals locations of the outer boundary of FSL on July 15, 2016 (Figure 13a) which is in a very good agreement with in situ salinity measurements performed on July 18–25, 2016, that is, 3–10 days after the satellite observations (Figure 11a). In August–September, FSL steadily expands. Its western boundary is located between the Yamal Peninsula and Novaya Zemlya,

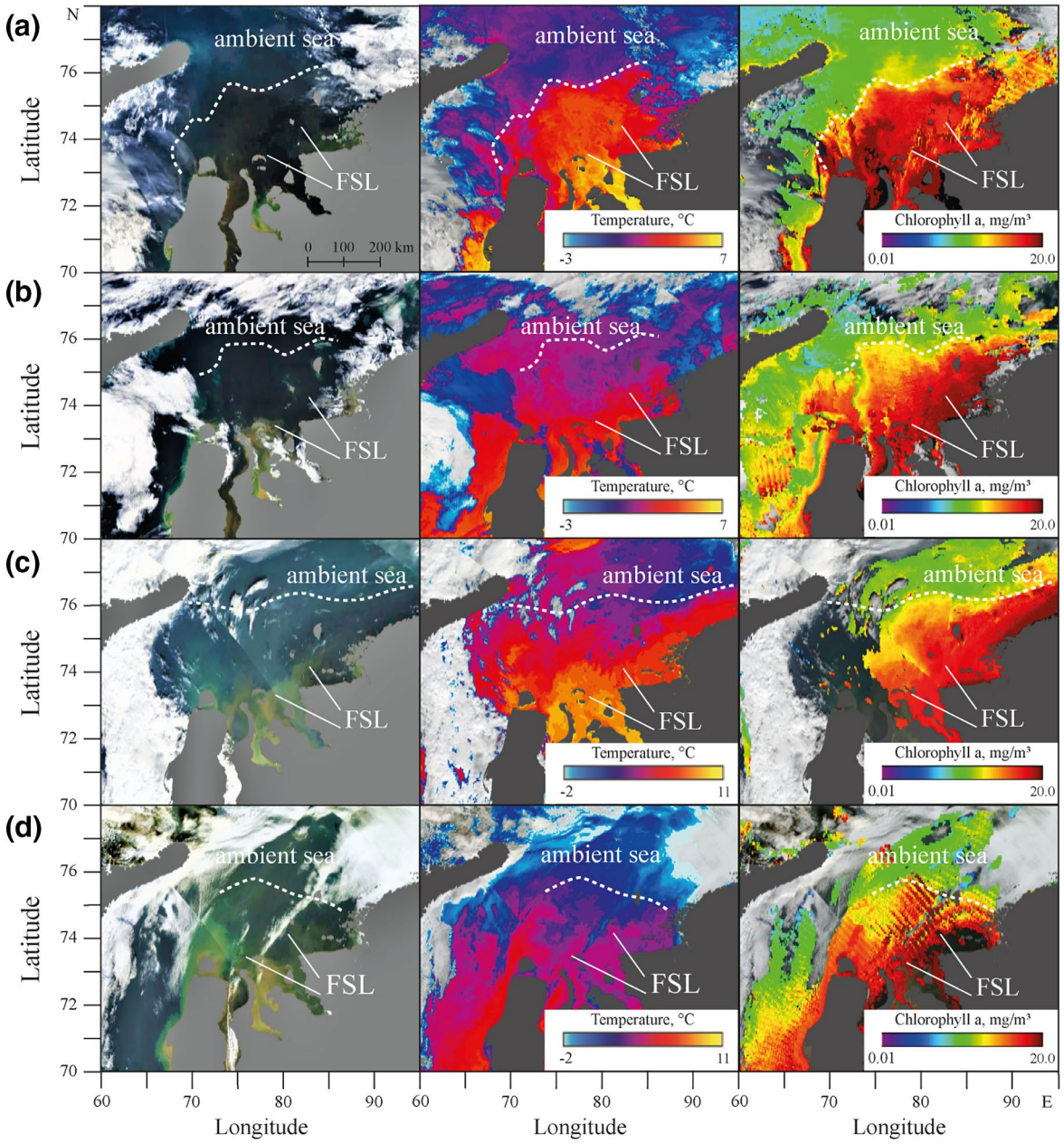

Figure 13. Corrected reflectance (left), brightness temperature (center), and Chl-a (right) from MODIS Terra/Aqua satellite images of the central Kara Sea acquired on (a) July 15, (b) August 15, (c) September 11, and (d) October 2, 2016. The dashed lines illustrate location of the outer border of FSL. FSL, freshened surface layer.

while its northern boundary stretches zonally from the north-eastern part of Novaya Zemlya. On August 15, 2016, the outer boundary of FSL shifted northward to the latitude of 75.5°N-76°N (Figure 13b), then on September 11, 2016 it reached the north-eastern part of Novaya Zemlya (Figure 13c). The eastern boundary of FSL, generally, is located on a distance of 150–200 km from the Yenisei Gulf during the ice-free season. However, during certain periods FSL forms a narrow current along the western coast of the Taymyr Peninsula. This current is spreading eastward from the central Kara Sea, in particular, it was observed at satellite imagery in the middle of September 2011. This narrow alongshore buoyancy current is a typical feature of river plumes and ROFI's (S. Y. Chao & Boicort, 1986; Fong & Geyer, 2002; Yankovsky & Chapman, 1997), in particular, its formation in the Kara Sea and propagation to the Laptev Sea was described by Janout

et al. (2015, 2017) and Osadchiev et al. (2020b). In October, the area of FSL decreases relative to its September extent. On October 2, 2016 its northern boundary shifted southward to the latitude of 75.5°N-76°N (Figure 13d).

4. Discussion

In situ measurements (Figures 6–12) and satellite observations (Figure 13) during ice-free periods show significant seasonal variability of the structure of FSL in the Kara Sea, while seasonal and interannual variability of its area and position is relatively low. This feature is not typical for other large river plumes (e.g., the Amazon [Lentz, 1995; Molleri et al., 2010], Congo [Y. Chao et al., 2015; Denamiel et al., 2013], Mississippi [Fournier et al., 2016; Walker, 1996], and Pearl [Dong et al., 2004; Xu et al., 2019] river plumes) and is caused by the formation of FSL during the relatively short freshet period in June–July. In June, the central Kara Sea is covered by ice and FSL experiences only low influence of wind forcing. July and August have the calmest wind forcing conditions throughout the year, in particular, the maximal registered number of days with strong wind (>15 m/s) in the central Kara Sea amounts to 4 in July and 5 in August, while the long-term mean values are 2 in July and 3 in August (Pavlov et al., 1996). As a result, in July–August, FSL occupies the same area in the semi-enclosed central Kara Sea between the Ob and Yenisei gulfs in the south, Taymyr Peninsula in the east and Novaya Zemlya in the northwest. In September and October, the intensity of wind forcing significantly increases, however, FSL is deep and large enough to remain relatively stable in response to wind forcing. As a result, strong and durable winds can induce shift of FSL westward (as was observed in September 2007), northward (September 2011), or eastward (October 2018), albeit the interannual variability of location of its western and northern boundaries is only 100–150 km.

In order to assess mixing of FSL, we calculated the vertical distribution of the freshwater fraction $F = (S_0\text{-}S)/S_0$ along the Ob and Yenisei transects, where S is the observed salinity, and $S_0 = 32$ is the reference ambient sea water salinity (Figure 3). The choice of the reference salinity was based on typical salinities of ambient saline sea water at the central Kara Sea (Johnson et al., 1997; Pavlov et al., 1996). F represents the volume fraction of freshwater in the surface layer that produced the observed salinity after mixing with ambient saline sea water (Nash et al., 2009). Then, based on the reconstructed distributions of F, we calculated the local freshwater content $L(x) = \int_{-b(x)}^{-s(x)} F(x,z)\,dz$ along the transects, that is, freshwater content in the water column, where x and z are the horizontal (along a transect) and vertical coordinates, respectively, $F(x, z)$ is the freshwater fraction at the point (x, z), $s(x)$, and $b(x)$ are the depths of the surface and bottom boundaries of the considered water mass. We calculated the local freshwater content in the plume (L_P), the ROFI (L_R), and the saline subjacent sea (L_S) (Figures 14 and 15). The ratio among these values along the transects is indicative of the local vertical distribution of freshwater among these water masses. Finally, we calculated the normalized total freshwater content along the transects $T = \frac{1}{l}\int_0^l L(x)\,dx$ in the plume (T_P), the ROFI (T_R), and the saline sea (T_S), where l is the length of the transect. These values are indicative of the volumes of freshwater contained in these water masses.

Figures 14 and 15 illustrate that the vertical distribution of freshwater fraction in the central Kara Sea is significantly different in July, August, and September. In July, flooding freshwater discharge forms the fresh and shallow Ob-Yenisei plume that spreads over wide area in the central Kara Sea (Figures 6a and 8a). Strong stratification between the plume and the subjacent sea decreases vertical mixing of the plume. As a result, the majority of the freshwater volume in the water column is concentrated within the fresh river plume, while almost no freshwater volume was contained within the ROFI and the ambient sea (Figures 14a and 15a). In July 2016, the local freshwater content in the plume exceeded the local freshwater content in the ROFI and the ambient sea along the whole spreading area of the plume. Total freshwater content within the plume (6.5 m) was 1 order of magnitude greater than total freshwater content within the ROFI (0.7 m) and the ambient sea (0.4 m).

In August and September, the vertical distribution of the freshwater fraction in the study area changes dramatically. Decreasing continental discharge rates to the Kara Sea and mixing of the plume with the ambient sea results in the formation of the ROFI in August (Figures 6b and 8b). As a result, a large share of the freshwater volume is transferred from the river plume to the ROFI. Freshwater volume in the subjacent sea also

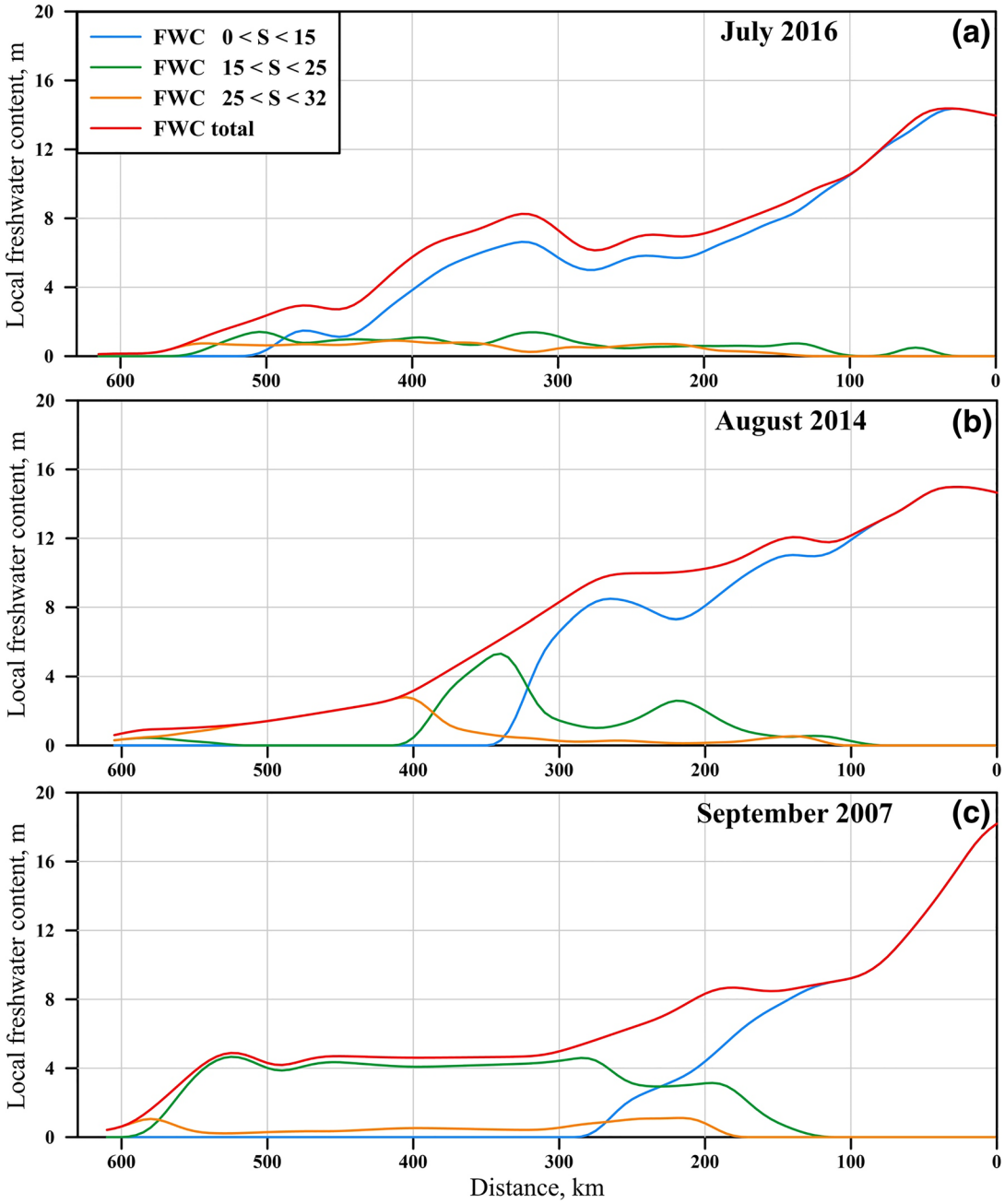

Figure 14. The local freshwater content (FWC) within the Ob-Yenisei plume (blue), the Kara ROFI (green), the ambient sea (orange) and in the whole water column (red) along the Ob transect in the Kara Sea on (a) July 18–21, 2016, (b) August 17–28, 2014, and (c) September 23–30, 2007. ROFI, regions of freshwater influence.

increases, albeit less abruptly. In particular, in August 2014 T_P decreased to 5.3 m, while T_R and T_S increased to 1.1 and 0.8 m, as compared to July 2016. The local freshwater content in the plume exceeded that of the ROFI at the southern part of the Ob transect, while the opposite situation was observed in the northern part of the Ob transect (Figure 14b). In September, dilution of FSL and transfer of the freshwater volume from the plume to the ROFI and from the ROFI to the subjacent sea accelerates. The plume dissipates in the open part of the sea (Figures 6c and 8c). As a result, the majority of the freshwater volume is contained within the ROFI (Figures 14c and 15c). Mixing of the ROFI with the subjacent sea, which also intensifies during this period, results in an increase of freshwater content below FSL and in the formation of the seasonal

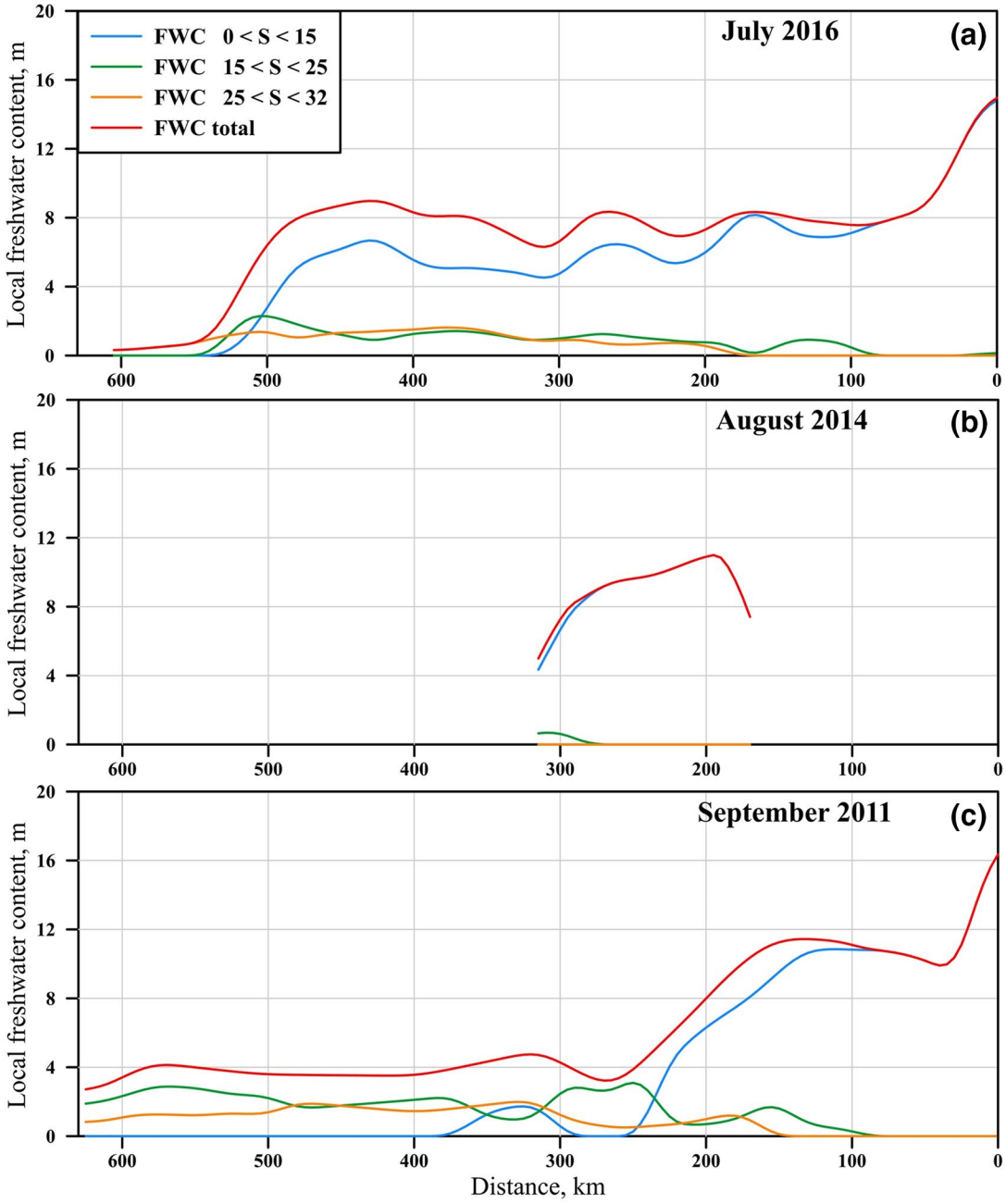

Figure 15. The local freshwater content (FWC) within the Ob-Yenisei plume (blue), the Kara ROFI (green), the ambient sea (orange), and in the whole water column (red) along the Yenisei transect in the Kara Sea on (a) July 24–25, 2016, (b) August 22–23, 2014, and (c) September 18–23, 2011. ROFI, regions of freshwater influence.

halocline. In September 2007 and September 2011, the local freshwater content in the ROFI exceeded the local freshwater content in the plume and the ambient sea along the transect except its most southernmost part. T_P decreased to 3.5 m, while T_R increased to 2.9 m, as compared to August 2014.

Vertical mixing plays the prevailing role in dilution of river plumes and ROFI's (Horner-Devine et al., 2015; Stacey et al., 2011; Yuan & Horner-Devine, 2013). Based on the reconstructed vertical distribution of freshwater fraction in the central Kara Sea in July 2016, August 2014, September 2007, and September 2011 we evaluated the vertical freshwater transport in the central Kara Sea during ice-free periods. The freshwater flux from the plume to the ROFI in July–August is represented by the equation

$\frac{T_P^A - T_P^J}{\Delta t_{JA}} = \frac{Q_O}{lb_O} + \frac{Q_Y}{lb_Y} - A_{z15}^{JA}\frac{1}{l}\int_0^l \frac{\partial F\left(x, z_{15}(x)\right)}{\partial z}dx$, where T_P^J and T_P^A are the values of T_P during the measurements in July and August, Δt_{JA} is the time period between these measurements, A_{z15}^{JA} is the average vertical eddy diffusivity across the boundary between the plume and the ROFI (defined by the isohaline of 15) during the time period Δt_{JA}, $z_{15}(x)$ is the vertical coordinate of the isohaline of 15, Q_O and Q_Y are the volumes of river discharge from the Ob and Yenisei gulfs during the time period Δt_{JA}, b_O, and b_Y are the widths of the Ob and Yenisei gulfs, l is the length of the transect, $F(x, z)$ is the freshwater fraction at the point (x, z). The left hand side of this equation stands for the difference in freshwater content within the plume between the measurements in July and August normalized by the time period between these measurements. The right hand side of this equation stands for the freshwater balance during this period, namely, the inflow of river water (the first term) and the downward flux from the plume to the ROFI (the second term). Horizontal advection is neglected in this equation justified by the stable position of FSL and the absence of significant freshwater sources besides the discharge from the Ob and Yenisei gulfs.

We obtain that average vertical eddy diffusivity

$$A_{z15}^{JA} = \left(\frac{Q_O}{lb_O} + \frac{Q_Y}{lb_Y} - \frac{T_P^A - T_P^J}{\Delta t_{JA}}\right)\frac{l}{\int_0^l \frac{\partial F\left(x, z_{15}(x)\right)}{\partial z}} \sim \left(\frac{3\cdot 10^4}{6\cdot 10^5 \cdot 4\cdot 10^4} + \frac{5\cdot 10^4}{6\cdot 10^5 \cdot 4\cdot 10^4} - \frac{5.3-6.5}{3283200}\right)\frac{6\cdot 10^5}{3.6\cdot 10^4}$$

$$\sim 6.8105\ \mathrm{m}^2/\mathrm{s}$$

which is indicative of the intensity of the average freshwater flux across the boundary between the plume and the ROFI in July–August. Similarly, we evaluate the freshwater flux across the boundary between the plume and the ROFI in August–September $A_{z15}^{AS} = 18.6\cdot 10^{-5}\ \mathrm{m}^2/\mathrm{s}$, as well as the values for the freshwater flux across the boundary between the ROFI and the subjacent saline sea in July–August $A_{z25}^{JA} = 2.9\cdot 10^{-5}\ \mathrm{m}^2/\mathrm{s}$ and in August–September $A_{z25}^{AS} = 3.2\cdot 10^{-5}\ \mathrm{m}^2/\mathrm{s}$. As a result, we show that the vertical flux of freshwater from FSL to the subjacent sea does not significantly change in July–September. On the other hand, this flux within FSL, that is, from the Ob-Yenisei plume to the Kara ROFI, dramatically increases from July to September caused by mixing of the plume and formation of the ROFI.

In order to quantify the role of horizontal mixing in dilution of the Ob-Yenisei plume and the Kara ROFI, we calculated average horizontal eddy diffusivity analogously to the corresponding vertical coefficients. The vertical and horizontal derivatives of the freshwater fraction F have the same order, while the integration length scales for the vertical (hundreds of kilometers) and horizontal (tens of meters) mixing differs by 4 orders. As a result, the intensity of lateral mixing is 4–5 orders of magnitude less, than the intensity of vertical mixing.

Wind and tidal forcing are the main mechanisms that induce mixing of river plumes and ROFI's with the subjacent saline sea water (Hetland, 2005; Horner-Devine et al., 2015; Juritsa et al., 2016). Wind-induced Ekman transport is the major mixing mechanism of FSL in the Kara Sea because the local tidal circulation is very weak. Velocities of tidal currents in the study area do not exceed 0.2 m/s, therefore, tidal mixing of FSL is negligible (Kagan et al., 2011; Osadchiev et al., 2020a). As a result, weak wind forcing in summer in the central Kara Sea is an important factor for the stability of the Ob-Yenisei plume and its relatively slow transformation to the Kara ROFI.

5. Conclusions

This work is focused on the FSL in the Kara Sea formed by large continental runoff. Based on in situ measurements, we study its horizontal and vertical structure during ice-free periods. We distinguish two different water masses within FSL, namely, the less saline (0–15) Ob-Yenisei river plume and the more saline (15–25) Kara ROFI. The Ob-Yenisei river plume is formed in June–July during the short-term flooding period of the Ob and Yenisei rivers. This plume spreads as a shallow and fresh water mass over a wide area in the central Kara Sea. Sharp salinity gradients form at the boundary between the plume and the subjacent saline sea. The zonal extent of the plume observed in the middle of July exceeded 250 km, while its area is estimated as 100,000–120,000 km^2.

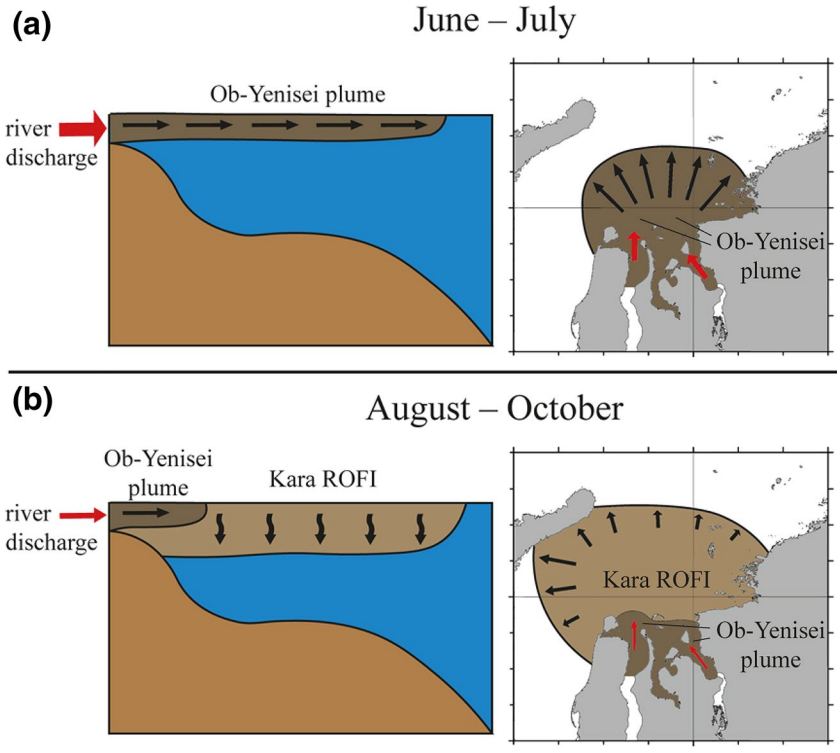

Figure 16. Schematic of transformation of FSL in the Kara Sea during ice-free periods, namely, horizontal advection of the Ob-Yenisei plume in (a) June–July and (b) formation of the Kara ROFI as a result of vertical mixing in August–October. FSL, freshened surface layer; ROFI, regions of freshwater influence.

After the end of the flooding period, the salinity of the surface layer decreases, while its depth increases due to mixing of the plume with subjacent saline sea water under low freshwater discharge conditions. As a result, in August the plume starts transforming into the more saline Kara ROFI bounded by distinct, however less sharp salinity gradients. This process occurs at the bottom and lateral boundaries of the plume, therefore, the northern boundary of the plume shifts southward, while the area of FSL remains stable. Finally, in late September–October the plume remains limited to the area adjacent to the Ob and Yenisei estuaries, while in the open part of the Kara Sea it totally transforms into the Kara ROFI. Zonal extent and area of the plume observed in late September–October were less than 50 km and 20,000 km^2, respectively. The Kara ROFI also mixes with the subjacent sea, which results in the accumulation of freshwater below FSL in August–September.

We consider the process of transformation of FSL during ice-free periods described above in context of the fate of freshwater discharge in the Kara Sea. Our results show that this process consists of two subsequent stages, namely, horizontal advection in summer and vertical mixing in autumn (Figure 16). Low discharge of the Ob and Yenisei rivers from autumn to spring results in the absence of FSL in the Kara Sea in spring (Harms & Karcher, 1999; Pavlov et al., 1996). Then a large volume of freshwater enters the Kara Sea during the period of flooding river discharge in June–July. Large salinity and pressure gradients are formed between the Ob-Yenisei plume and ambient sea due to the absence of residual FSL. It causes intense offshore spreading of the Ob-Yenisei plume and the formation of the thin and fresh FSL over a wide area in the Kara Sea (Figure 16a). The intense expanding of FSL slows down in August as a result of decreasing of freshwater discharge. It occupies relatively stable area in the central Kara Sea and steadily mixes with the subjacent sea (Figure 16b). As a result, downward freshwater transport and formation of the seasonal halocline occurs in August–October at the stable area located in the central Kara Sea. Finally, FSL dissipates in winter (Pavlov et al., 1996).

The Ob and Yenisei rivers have very large seasonal variability of river discharge with low runoff during the majority of a year followed by short and intense summer floods. Similar annual discharge regimes are

observed for other rivers that inflow to the Arctic Ocean, for example, the Lena, Kolyma, Mackenzie, Indigirka, etc. Thus, the pattern of formation and dissipation of FSL in the Kara Sea reported in this work can be the case for other FSLs formed by large rivers in the Arctic Ocean. The related studies are essential for the assessment of large-scale freshwater transport in the Arctic Ocean which plays a key role in stratification and ice formation, as well as in many physical, biological, and geochemical processes (E. C. Carmack et al., 2016; Nummelin et al., 2016).

The Kara Sea is low productive as compared to the neighboring Barents Sea due to the influence of the high river discharge (E. Carmack et al., 2006; Demidov et al., 2014a; Sakshaug, 2004). The formation of large and stratified FSL in the Kara Sea inhibits vertical water exchange and, therefore, hinders nutrient supply to the euphotic zone from the nutrient-rich deep waters (Demidov et al., 2014a, 2014b; Mosharov, 2010). The high turbidity of FSL and small depth of the euphotic zone also negatively affect primary production in the central Kara Sea (Demidov et al., 2018). As a result, the discharge from the Ob and Yenisei rivers during the summer freshet period does not induce intense spring algae bloom in the Kara Sea (Mosharov et al., 2018a). On the opposite, the formation of large and stable FSL in June–July is an important factor explaining the low productivity of the Kara Sea.

The Arctic Ocean is strongly affected by the ongoing climate change. Total annual river runoff to the Arctic Ocean (including the discharge to the Kara Sea) significantly increased during the 21st century (Peterson et al., 2002) and is predicted to continue to increase in the 21st century (Haine et al., 2015; Lehner et al., 2012). Generally, the increase of discharge of the Ob and Yenisei rivers will increase stratification of FSL in the Kara Sea (Nummelin et al., 2016) and potentially will increase its area. However, changes in the hydrological regime of these rivers can be even more important than increases of the net freshwater discharge. The observed increase in annual runoff of these rivers during the last decades was formed mainly by the increase of discharge during the winter-spring period, while discharge during the flooding period remained almost the same (Polukhin, 2019). Therefore, the existing pattern of formation and dissipation of FSL in the Kara Sea will change only in case of significant future increase of winter-spring discharge and flattening of the summer flooding period. On the other hand, in case of future increase of intensity and/or duration of summer freshet discharge the Ob-Yenisei plume will be more stable and its transformation to the Kara ROFI will occur later. This process can accelerate ice formation in the central Kara Sea. Earlier ice retreat in the central Kara Sea which is also forecasted in the near future will result in increased wind-induced mixing of FSL and will support earlier formation of the Kara ROFI. Therefore, the processes discussed above are characterized by complex relations and feedbacks and require specific numerical modeling studies.

Data Availability Statement

The ERA5 reanalysis data were downloaded from the European Centre for Medium-Range Weather Forecasts (ECMWF) website https://www.ecmwf.int/en/forecasts/datasets/archive-datasets/reanalysis-datasets/era5. The MODIS Terra and Aqua satellite data were downloaded from the NASA repository of the satellite data https://ladsweb.modaps.eosdis.nasa.gov/. The river discharge data were downloaded from the Arctic Great Rivers Observatory (ArcticGRO) website https://www.arcticrivers.org/data. The sea ice data were downloaded from the Arctic and Antarctic Research Institute (AARI) website http://www.aari.ru/odata/_d0015.php?mod=1. The in situ data are available in supplementary information.

Acknowledgments
This research was funded by the Ministry of Science and Higher Education of the Russian Federation, theme 0149-2019-0003 (collecting and processing of meteorological data); the Russian Foundation for Basic Research, research projects 18-05-60302 (collecting and processing of in situ data), 18-05-60069 (collecting and processing of satellite data), 20-35-70039 (study of freshwater transport), and 18-05-00019 (study of river plumes).

References

Aagaard, K., & Carmack, E. C. (1989). The role of sea ice and other fresh water in the Arctic circulation. *Journal of Geophysical Research*, *94*, 14485–14498. https://doi.org/10.1029/JC094iC10p14485

Asadulin, E. E., Miroshnikov, A. Y, Usacheva, A. A., & Velichkin, V. I. (2015). Geochemical recognition of terrigenous material from the Ob and Yenisei rivers in bottom sediments of the eastern part of the Kara Sea. *Doklady Earth Sciences*, *461*, 270–272. https://doi.org/10.1134/S1028334X15030095

Asadulin, E. E., Miroshnikov, A. Y, & Velichkin, V. I. (2013). Geochemical signature of bottom sediments in the mixing zones of Ob and Yenisei waters with Kara Sea water. *Geochemistry International*, *51*, 1005–1018. https://doi.org/10.1134/S0016702913120021

Carmack, E., Barber, D., Christensen, J., Macdonald, R., Rudels, B., & Sakshaug, E. (2006). Climate variability and physical forcing of the food webs and the carbon budget on panarctic shelves. *Progress in Oceanography*, *71*, 145–181. https://doi.org/10.1016/j.pocean.2006.10.005

Carmack, E. C., Yamamoto-Kawai, M., Haine, T. W., Bacon, S., Bluhm, B. A., Lique, C., et al. (2016). Freshwater and its role in the Arctic Marine System: Sources, disposition, storage, export, and physical and biogeochemical consequences in the Arctic and global oceans. *Journal of Geophysical Research: Biogeosciences*, *121*, 675–717. https://doi.org/10.1002/2015JG003140

Chao, S. Y., & Boicort, W. G. (1986). Onset of estuarine plumes. *Journal of Physical Oceanography*, *16*, 2137–2149. https://doi.org/10.1175/1520-0485(1986)016<2137:OOEP>2.0.CO;2

Chao, Y., Farrara, J. D., Schumann, G., Andreadis, K. M., & Moller, D. (2015). Sea surface salinity variability in response to the Congo river discharge. *Continental Shelf Research*, *99*, 35–45. https://doi.org/10.1016/j.csr.2015.03.005

Demidov, A. B., Gagarin, V. I., Vorobieva, O. V., Makkaveev, P. N., Artemiev, V. A., Khrapko, A. N., et al. (2018). Spatial and vertical variability of primary production in the Kara Sea in July and August 2016: The influence of the river plume and subsurface chlorophyll maxima. *Polar Biology*, *41*, 563–578. https://doi.org/10.1007/s00300-017-2217-x

Demidov, A. B., Mosharov, S. A., & Makkaveev, P. N. (2014a). Patterns of the Kara Sea primary production in autumn: Biotic and abiotic forcing of subsurface layer. *Journal of Marine Systems*, *132*, 130–149. https://doi.org/10.1016/j.jmarsys.2014.01.014

Demidov, A. B., Mosharov, S. A., & Makkaveev, P. N. (2014b). Evaluation of the influence of abiotic and biotic factors on primary production in the Kara Sea in autumn. *Oceanology*, *55*, 535–546. https://doi.org/10.1134/S0001437015040037

Denamiel, C., Budgell, W. P., & Toumi, R. (2013). The Congo River plume: Impact of the forcing on the far-field and near-field dynamics. *Journal of Geophysical Research: Oceans*, *118*, 964–989. https://doi.org/10.1002/jgrc.20062

Dmitrenko, I. A., Rudels, B., Kirillov, S. A., Aksenov, Y. O., Lien, V. S., Ivanov, V. V., et al. (2015). Atlantic water flow into the Arctic Ocean through the St. Anna Trough in the northern Kara Sea. *Journal of Geophysical Research: Oceans*, *120*, 5158–5178. https://doi.org/10.1002/2015JC010804

Dolgopolova, E. N. (2015). Regularities in the motion of water and sediments at the mouth of a river of estuarine-deltaic type: Case study of the Yenisei River. *Water Research*, *42*, 198–207. https://doi.org/10.1134/s0097807815020050

Dong, L., Su, J., Wong, L. A., Cao, Z., & Chen, J. C. (2004). Seasonal variation and dynamics of the Pearl River plume. *Continental Shelf Research*, *24*, 1761–1777. https://doi.org/10.1016/j.csr.2004.06.006

Dubinina, E. O., Kossova, S. A., Miroshnikov, A. Y., & Kokryatskaya, N. M. (2017a). Isotope parameters (δD, $\delta^{18}O$) and sources of freshwater input to the Kara Sea. *Oceanology*, *57*, 31–40. https://doi.org/10.1134/S0001437017010040

Dubinina, E. O., Kossova, S. A., Miroshnikov, A. Y., & Kokryatskaya, N. M. (2017b). Isotope (δD, $\delta^{18}O$) systematics in waters of the Russian Arctic seas. *Geochemistry International*, *55*, 1022–1032. https://doi.org/10.1134/S0016702917110052

Fichot, C., Kaiser, K., Hooker, S. B., Amon, R. M. W., Babin, M., Belanger, S., et al. (2013). Pan-Arctic distributions of continental runoff in the Arctic Ocean. *Scientific Reports*, *3*, 1053. https://doi.org/10.1038/srep01053

Fong, D. A., & Geyer, W. R. (2002). The alongshore transport of freshwater in a surface-trapped river plume. *Journal of Physical Oceanography*, *32*, 957–972. https://doi.org/10.1175/1520-0485(2002)032<0957:TATOFI>2.0.CO;2

Fournier, S., Lee, T., & Gierach, M. M. (2016). Seasonal and interannual variations of sea surface salinity associated with the Mississippi River plume observed by SMOS and Aquarius. *Remote Sensing Environment*, *180*, 431–439. https://doi.org/10.1016/j.rse.2016.02.050

Galimov, E. M., Kodina, L. A., Stepanets, O. V., & Korobeinik, G. S. (2006). Biogeochemistry of the Russian Arctic. Kara Sea: Research results under the SIRRO project, 1995–2003. *Geochemistry International*, *44*, 1053–1104. https://doi.org/10.1134/s0016702906110012

Gebhardt, A. C., Gaye-Haake, B., Unger, D., Lahajnar, N., & Ittekkot, V. (2004). Recent particulate organic carbon and total suspended matter fluxes from the Ob and Yenisei Rivers into the Kara Sea (Siberia). *Marine Geology*, *207*, 225–245. https://doi.org/10.1016/j.margeo.2004.03.010

Geyer, W. R., Beardsley, R. C., Lentz, S. J., Candela, J., Limeburner, R., Johns, W. E., et al. (1996). Physical oceanography of the Amazon shelf. *Continental Shelf Research*, *16*, 575–616. https://doi.org/10.1016/0278-4343(95)00051-8

Glukhovets, D. I., & Goldin, Y. A. (2014). A study of bio-optical characteristics of waters of the Kara Sea by using data of satellite and ship measurements. *Current Problems in Remote Sensing of the Earth from Space*, *11*, 346–350.

Glukhovets, D. I., & Goldin, Y. A. (2020). Surface desalinated layer distribution in the Kara Sea determined by shipboard and satellite data. *Oceanologia*, *62*, 364–373. https://doi.org/10.1016/j.oceano.2020.04.002

Gordeev, V. V., Martin, J. M., Sidorov, J. S., & Sidorova, M. V. (1996). A reassessment of the Eurasian river input of water, sediment, major elements, and nutrients to the Arctic Ocean. *American Journal of Science*, *296*, 664–691. https://doi.org/10.2475/ajs.296.6.664

Haine, T. W., Curry, B., Gerdes, R., Hansen, E., Karcher, M., Lee, C., et al. (2015). Arctic freshwater export: Status, mechanisms, and prospects. *Global and Planetary Change*, *125*, 13–35. https://doi.org/10.1016/j.gloplacha.2014.11.013

Harms, I. H., & Karcher, M. J. (1999). Modeling the seasonal variability of circulation and hydrography in the Kara Sea. *Journal of Geophysical Research*, *104*(C6), 13431–13448. https://doi.org/10.1029/1999jc900048

Harms, I. H., & Karcher, M. J. (2005). Kara Sea freshwater dispersion and export in the late 1990s. *Journal of Geophysical Research*, *110*, C08007. https://doi.org/10.1029/2004jc002744

Hetland, R. D. (2005). Relating river plume structure to vertical mixing. *Journal of Physical Oceanography*, *35*, 1667–1688. https://doi.org/10.1175/JPO2774.1

Horner-Devine, A. R., Hetland, R. D., & MacDonald, D. G. (2015). Mixing and transport in coastal river plumes. *Annual Review of Fluid Mechanics*, *47*, 569–594. https://doi.org/10.1146/annurev-fluid-010313-141408

Janout, M. A., Aksenov, Y., Hölemann, J. A., Rabe, B., Schauer, U., Polyakov, I. V., et al. (2015). Kara Sea freshwater transport through Vilkitsky Strait: Variability, forcing, and further pathways toward the western Arctic Ocean from a model and observations. *Journal of Geophysical Research: Oceans*, *120*, 4925–4944. https://doi.org/10.1002/2014JC010635

Janout, M. A., Hölemann, J.A., Timokhov, L., Gutjahr, O., & Heinemann, G. (2017). Circulation in the northwest Laptev Sea in the eastern Arctic Ocean: Crossroads between Siberian River water, Atlantic water and polynya-formed dense water. *Journal of Geophysical Research: Oceans*, *122*(8), 6630–6647. http://dx.doi.org/10.1002/2017jc013159

Johnson, D. R., McClimans, T. A., King, S., & Grenness, T. (1997). Fresh water masses in the Kara Sea during summer. *Journal of Marine Systems*, *12*, 127–145. https://doi.org/10.1016/s0924-7963(96)00093-0

Jurisa, J. T., Nash, J. D., Moum, J. N., & Kilcher, L. F. (2016). Controls on turbulent mixing in a strongly stratified and sheared tidal river plume. *Journal of Physical Oceanography*, *46*, 2373–2388. https://doi.org/10.1175/JPO-D-15-0156.1

Kagan, B. A., Sofina, E. V., & Timofeev, A. A. (2011). Modeling of the M2 surface and internal tides and their seasonal variability in the Arctic Ocean: Dynamics, energetics and tidally induced diapycnal diffusion. *Journal of Marine Research*, *69*, 245–276. https://doi.org/10.1357/002224011798765312

Kohler, H., Meon, B., Gordeev, V. V., Spitzy, A., & Amon, R. M. W. (2003). Dissolved organic matter (DOM) in the estuaries of Ob and Yenisei and the adjacent Kara Sea, Russia. In R. Stein, K. Fahl, D.K. Futterer, E.M. Galimov, & O.V. Stepanets (Eds.), *Proceedings in marine science* (Vol. *6*, pp. 281–308). Amsterdam, The Netherlands: Elsevier.

Korotkina, O. A., Zavialov, P. O., & Osadchiev, A. A. (2011). Submesoscale variability of the current and wind fields in the coastal region of Sochi. *Oceanology*, *51*, 745–754. https://doi.org/10.1134/s0001437011050109

Korotkina, O. A., Zavialov, P. O., & Osadchiev, A. A. (2014). Synoptic variability of currents in the coastal waters of Sochi. *Oceanology*, *54*, 545–556. https://doi.org/10.1134/s0001437014040079

Kubryakov, A., Stanichny, S., & Zatsepin, A. (2016). River plume dynamics in the Kara Sea from altimetry-based Lagrangian model, satellite salinity and chlorophyll data. *Remote Sensing of Environment*, *176*, 177–187. https://doi.org/10.1016/j.rse.2016.01.020

Lambert, E., Nummelin, A., Pemberton, P., & Ilıcak, M. (2019). Tracing the imprint of river runoff variability on Arctic water mass transformation. *Journal of Geophysical Research: Oceans*, *124*, 302–319. https://doi.org/10.1029/2017JC013704

Lehner, F., Raible, C. C., Hofer, D., & Stocker, T. F. (2012). The freshwater balance of polar regions in transient simulations from 1500 to 2100 AD using a comprehensive coupled climate model. *Climate Dynamics*, *39*, 347–363. https://doi.org/10.1007/s00382-011-1199-6

Lentz, S. J. (1995). Seasonal variations in the horizontal structure of the Amazon Plume inferred from historical hydrographic data. *Journal of Geophysical Research*, *100*, 2391–2400. https://doi.org/10.1029/94JC01847

Levitan, M. A., Bourtman, M. V., Demina, L. L., Chudetsky, M. Y., & Schoster, F. (2005). Facies variability of surface sediments from the Ob-Yenisei shoal and the Ob and Yenisei estuaries. *Lithology and Mineral Resources*, *40*, 408–419. https://doi.org/10.1007/s10987-005-0039-3

Lewis, K. M., & Arrigo, K. R. (2020). Ocean color algorithms for estimating chlorophyll a, CDOM absorption, and particle backscattering in the Arctic Ocean. *Journal of Geophysical Research: Oceans*, *125*, e2019JC015706. https://doi.org/10.1029/2019JC015706

Makkaveev, P. N., Melnikova, Z. G., Polukhin, A. A., Stepanova, S. V., Khlebopashev, P. V., & Chulcova, A. L. (2015). Hydrochemical characteristics of the waters of the western part of the Kara Sea. *Oceanology*, *55*, 485–496. https://doi.org/10.1134/s0001437015040116

McClimans, T. A., Johnson, D. R., Krosshavn, M., King, S. E., Carroll, J., & Grenness, T. (2000). Transport processes in the Kara Sea. *Journal of Geophysical Research*, *105*(C6), 14121–14139. https://doi.org/10.1029/1999jc000012

Miroshnikov, A. Y. (2013). Radiocaesium distribution in the bottom sediments of the Kara Sea. *Water Research*, *40*, 723–732. https://doi.org/10.1134/S0097807813070105

Molleri, G. S., Novo, E. M. D. M., & Kampel, M. (2010). Space-time variability of the Amazon River plume based on satellite ocean color. *Continental Shelf Research*, *30*, 342–352. https://doi.org/10.1016/j.csr.2009.11.015

Morozov, E. G., Paka, V. T., & Bakhanov, V. V. (2008). Strong internal tides in the Kara Gates Strait. *Geophysical Research Letters*, *35*, L16603. https://doi.org/10.1029/2008GL033804

Morozov, E. G., Parrilla-Barrera, G., Velarde, M. G., & Scherbinin, A. D. (2003). The straits of Gibraltar and Kara Gates: A comparison of internal tides. *Oceanologica Acta*, *26*, 231–241. https://doi.org/10.1016/S0399-1784(03)00023-9

Mosharov, S. A. (2010). Distribution of the primary production and chlorophyll a in the Kara Sea in September of 2007. *Oceanology*, *50*, 884–892. https://doi.org/10.1134/S0001437010060081

Mosharov, S. A., Sazhin, A. F., Druzhkova, E. I., & Khlebopashev, P. V. (2018a). Structure and productivity of the phytocenosis in the southwestern Kara Sea in early spring. *Oceanology*, *58*, 396–404. https://doi.org/10.1134/S0001437018030141

Mosharov, S. A., Sergeeva, V. M., Kremenetskiy, V. V., Sazhin, A. F., & Stepanova, S. V. (2018b). Assessment of phytoplankton photosynthetic efficiency based on measurement of fluorescence parameters and radiocarbon uptake in the Kara Sea. *Estuarine, Coastal and Shelf Science*, *218*, 59–69. https://doi.org/10.1016/j.ecss.2018.12.004

Nash, J. D., Kilcher, L. F., & Moum, J. N. (2009). Structure and composition of a strongly stratified, tidally pulsed river plume. *Journal of Geophysical Research*, *114*, C00B12. https://doi.org/10.1029/2008JC005036

Nummelin, A., Ilicak, M., Li, C., & Smedsrud, L. H. (2016). Consequences of future increased Arctic runoff on Arctic Ocean stratification, circulation, and sea ice cover. *Journal of Geophysical Research: Oceans*, *121*, 617–637. https://doi.org/10.1002/2015JC011156

O'Reilly, J. E., Maritorena, S., Mitchell, B. G., Siegel, D. A., Carder, K. L., Garver, S. A., et al. (1998). Ocean color chlorophyll algorithms for SeaWiFS. *Journal of Geophysical Research*, *103*, 24937–24953. https://doi.org/10.1029/98JC02160

Osadchiev, A. A. (2015). A method for quantifying freshwater discharge rates from satellite observations and Lagrangian numerical modeling of river plumes. *Environmental Research Letters*, *10*, 085009. https://doi.org/10.1088/1748-9326/10/8/085009

Osadchiev, A. A. (2017). Spreading of the Amur river plume in the Amur Liman, the Sakhalin Gulf, and the Strait of Tartary. *Oceanology*, *57*, 376–382. https://doi.org/10.1134/S0001437017020151

Osadchiev, A. A. (2018). Small mountainous rivers generate high-frequency internal waves in coastal ocean. *Scientific Reports*, *8*, 16609. https://doi.org/10.1038/s41598-018-35070-7

Osadchiev, A. A., Asadulin, E. E., Miroshnikov, A. Y., Zavialov, I. B., Dubinina, E. O., & Belyakova, P. A. (2019). Bottom sediments reveal inter-annual variability of interaction between the Ob and Yenisei plumes in the Kara Sea. *Scientific Reports*, *9*, 18642. https://doi.org/10.1038/s41598-019-55242-3

Osadchiev, A. A., Izhitskiy, A. S., Zavialov, P. O., Kremenetskiy, V. V., Polukhin, A. A., Pelevin, V. V., & Toktamysova, Z. M. (2017). Structure of the buoyant plume formed by Ob and Yenisei river discharge in the southern part of the Kara Sea during summer and autumn. *Journal Geophysical Research: Oceans*, *122*, 5916–5935. https://doi.org/10.1002/2016JC012603

Osadchiev, A. A., Korotenko, K. A., Zavialov, P. O., Chiang, W.-S., & Liu, C.-C. (2016). Transport and bottom accumulation of fine river sediments under typhoon conditions and associated submarine landslides: Case study of the Peinan River, Taiwan. *Natural Hazards and Earth System Sciences*, *16*, 41–54. https://doi.org/10.5194/nhess-16-41-2016

Osadchiev, A. A., Medvedev, I. P., Shchuka, S. A., Kulikov, M. E., Spivak, E. A., Pisareva, M. A., & Semiletov, I. P. (2020a). Influence of estuarine tidal mixing on structure and spatial scales of large river plumes. *Ocean Science*, *16*, 1–18. https://doi.org/10.5194/os-16-1-2020

Osadchiev, A. A., Pisareva, M. N., Spivak, E. A., Shchuka, S. A., & Semiletov, I. P. (2020b). Freshwater transport between the Kara, Laptev, and East-Siberian seas. *Scientific Reports*, *10*, 13041. https://doi.org/10.1038/s41598-020-70096-w

Osadchiev, A. A., Silvestrova, K. P., & Myslenkov, S. A. (2020c). Wind-driven coastal upwelling near large river deltas in the Laptev and East-Siberian seas. *Remote Sensing*, *12*, 844. https://doi.org/10.3390/rs12050844

Osadchiev, A. A., Barymova, A. A., Sedakov, R. O., Zhiba, R. Y., & Dbar, R. S. (2020d). Spatial structure, short-temporal variability, and dynamical features of small river plumes as observed by aerial drones: Case study of the Kodor and Bzyp river plumes. *Remote Sensing*, *12*, 3079. https://doi.org/10.3390/rs12183079

Osadchiev, A. A., & Sedakov, R. O. (2019). Spreading dynamics of small river plumes off the northeastern coast of the Black Sea observed by Landsat 8 and Sentinel-2. *Remote Sensing of Environment*, *221*, 522–533. https://doi.org/10.1016/j.rse.2018.11.043

Osadchiev, A. A., & Zavialov, P. O. (2020). Structure and dynamics of plumes generated by small rivers. In J. Pan (Ed.), *Estuaries and coastal zones - Dynamics and response to environmental changes* (pp. 125-144). London, UK: IntechOpen. https://doi.org/10.5772/intechopen.87843

Ostrander, C. E., McManus, M. A., Decarlo, E. H., & Mackenzie, F. T. (2008). Temporal and spatial variability of freshwater plumes in a semi-enclosed Estuarine–Bay System. *Estuaries and Coasts*, *31*, 192–203. https://doi.org/10.1007/s12237-007-9001-z

Panteleev, G., Proshutinsky, A., Kulakov, M., Nechaev, D. A., & Maslowski, W. (2007). Investigation of the summer Kara Sea circulation employing a variational data assimilation technique. *Journal of Geophysical Research*, *112*, C04S15. https://doi.org/10.1029/2006JC003728

Pavlov, V. K., & Pfirman, S. L. (1995). Hydrographic structure and variability of the Kara Sea: Implications for pollutant distribution. *Deep Sea Research Part II: Tropical Studies in Oceanography*, *42*, 1369–1390. https://doi.org/10.1016/0967-0645(95)00046-1

Pavlov, V. K., Timokhov, L. A., Baskakov, G. A., Kulakov, M. Yu, Kurazhov, V. K., Pavlov, P. V., et al. (1996). *Hydrometeorological regime of the Kara, Laptev, and East-Siberian seas*. Technical Memorandum, APL-UW TM 1-96. Applied Physics Laboratory, University of Washington.

Peterson, B. J., Holmes, R. M., McClelland, J. W., Vorosmarty, C. J., Lammers, R. B., Shiklomanov, A. I., et al. (2002). Increasing river discharge to the Arctic Ocean. *Science*, *298*, 2171–2173. https://doi.org/10.1126/science.1077445

Polukhin, A. A. (2019). The role of river runoff in the Kara Sea surface layer acidification and carbonate system changes. *Environmental Research Letters*, *14*, 105007. https://doi.org/10.1088/1748-9326/ab421

Romanova, N. D., & Boltenkova, M. A. (2020). Seasonal variability of bacterioplankton of the Yenisei estuary. *Oceanology*, *60*, 74–82. https://doi.org/10.1134/S0001437020010191

Romero, L., Siegel, D. A., McWilliams, J. C., Uchiyama, Y., & Jones, C. (2016). Characterizing storm water dispersion and dilution from small coastal streams. *Journal of Geophysical Research: Oceans*, *121*, 3926–3943. https://doi.org/10.1002/2015JC011323

Sakshaug, E. (2004). Primary and secondary production in the Arctic Seas. In R. Stein & R. W. MacDonald (Eds.), *The organic cccycle in the Arctic Ocean* (pp. 57–81). Berlin, Heidelberg: Springer. https://doi.org/10.1007/978-3-642-18912-8_3

Schiller, R. V., Kourafalou, V. H., Hogan, P., & Walker, W. D. (2011). The dynamics of the Mississippi River plume: Impact of topography, wind and offshore forcing on the fate of plume waters. *Journal of Geophysical Research*, *116*, C06029. https://doi.org/10.1029/2010JC006883

Semizhon, T., Rollin, S., Spasova, Y., & Klemt, E. (2010). Transport and distribution of artificial gamma-emitting radionuclides in the River Yenisei and its sediment. *Journal of Environmental Radioactivity*, *101*, 385–402. https://doi.org/10.1016/j.jenvrad.2010.02.012

Stacey, M. T., Rippeth, T. P., & Nash, J. D. (2011). Turbulence and stratification in estuaries and coastal seas. In E. Wolanski & D. McLusky (Eds.), Treatise on estuarine and coastal Science (Vol *2*, pp. 9–35). Amsterdam, The Netherlands: Elsevier. https://doi.org/10.1016/B978-0-12-374711-2.00204-7

Unger, D., Gaye-Haake, B., Neumann, K., Gebhardt, A. C., & Ittekkot, V. (2005). Biogeochemistry of suspended and sedimentary material in the Ob and Yenisei rivers and Kara Sea: Amino acids and amino sugars. *Continental Shelf Research*, *25*, 437–460. https://doi.org/10.1016/j.csr.2004.09.014

Walker, N. D. (1996). Satellite assessment of Mississippi River plume variability: Causes and predictability. *Remote Sensing of Environment*, *58*, 21–35. https://doi.org/10.1016/0034-4257(95)00259-6

Werdell, P. J., & Bailey, S. W. (2005). An improved bio-optical data set for ocean color algorithm development and satellite data product validation. *Remote Sensing of Environment*, *98*, 122–140. https://doi.org/10.1016/j.rse.2005.07.001

Williams, W. J., & Carmack, E. C. (2015). The 'interior' shelves of the Arctic Ocean: Physical oceanographic setting, climatology and effects of sea-ice retreat on cross-shelf exchange. *Progress in Oceanography*, *139*, 24–31. https://doi.org/10.1016/j.pocean.2015.07.008

Xu, C., Xu, Y., Hu, J., Li, S., & Wang, B. (2019). A numerical analysis of the summertime Pearl River plume from 1999 to 2010: Dispersal patterns and intraseasonal variability. *Journal of Marine Systems*, *192*, 15–27. https://doi.org/10.1016/j.jmarsys.2018.12.010

Yankovsky, A. E., & Chapman, D. C. (1997). A simple theory for the fate of buoyant coastal discharges. *Journal of Physical Oceanography*, *27*, 1386–1401. https://doi.org/10.1175/1520-0485(1997)027<1386:astftf>2.0.co;2

Yuan, Y., & Horner-Devine, A. R. (2013). Laboratory investigation of the impact of lateral spreading on buoyancy flux in a river plume. *Journal of Physical Oceanography*, *43*, 2588–2610. https://doi.org/10.1175/JPO-D-12-0117.1

Zatsepin, A. G., Kremenetskiy, V. V., Kubryakov, A. A., Stanichny, S. V., & Soloviev, D. M. (2015). Propagation and transformation of waters of the surface desalinated layer in the Kara Sea. *Oceanology*, *55*, 450–460. https://doi.org/10.1134/s0001437015040153

Zatsepin, A. G., Morozov, E. G., Paka, V. T., Demidov, A. N., Kondrashov, A. A., Korzh, A. O., et al. (2010a). Circulation in the southwestern part of the Kara Sea in September 2007. *Oceanology*, *50*, 643–656. https://doi.org/10.1134/S0001437010050024

Zatsepin, A. G., Zavialov, P. O., Kremenetskiy, V. V., Poyarkov, S. G., & Soloviev, D. M. (2010b). The upper desalinated layer in the Kara Sea. *Oceanology*, *50*, 657–667. https://doi.org/10.1134/s0001437010050036

Zavialov, P. O., Izhitskiy, A. S., Osadchiev, A. A., Pelevin, V. V., & Grabovskiy, A. B. (2015). The structure of thermohaline and bio-optical fields in the upper layer of the Kara Sea in September 2011. *Oceanology*, *55*, 461–471. https://doi.org/10.1134/s0001437015040177

Zavialov, P. O., Pelevin, V. V., Belyaev, N. A., Izhitskiy, A. S., Konovalov, B. V., Krementskiy, V. V., et al. (2018). High resolution LiDAR measurements reveal fine internal structure and variability of sediment-carrying coastal plume. *Estuarine, Coastal and Shelf Science*, *205*, 40–45. https://doi.org/10.1016/j.ecss.2018.01.008